

Numerical Continuation of Invariant Solutions of the Complex Ginzburg-Landau Equation

Vanessa López[†]

June 15, 2022

Abstract

We consider the problem of computation and deformation of group orbits of solutions of the complex Ginzburg-Landau equation (CGLE) with cubic nonlinearity in $1+1$ space-time dimension invariant under the action of the three-dimensional Lie group of symmetries $A(x, t) \rightarrow e^{i\theta} A(x + \sigma, t + \tau)$. From an initial set of group orbits of such invariant solutions, for a particular point in the parameter space of the CGLE, we obtain new sets of group orbits of invariant solutions via numerical continuation along paths in the moduli space. The computed solutions along the continuation paths are unstable, and have multiple modes and frequencies active in their spatial and temporal spectra, respectively. Structural changes in the moduli space resulting in symmetry gaining / breaking associated mainly with the spatial reflection symmetry $A(x, t) \rightarrow A(-x, t)$ of the CGLE were frequently uncovered in the parameter regions traversed.

Key Words: invariant solutions, relative periodic orbits, complex Ginzburg-Landau equation, continuous symmetries, numerical continuation

1 Introduction

We consider the problem of numerical computation and deformation of solutions of evolutionary partial differential equations (PDEs) fixed by the action of a Lie group $\Gamma = \Gamma_1 \times \mathbb{R}$ of continuous symmetries of the PDEs, where \mathbb{R} is the group of time translations and Γ_1 is non-trivial. Within this context, such *invariant solutions* are also known as *relative periodic orbits* or *relative time-periodic solutions* of an (autonomous) *equivariant dynamical system*. In this paper, we work with the complex Ginzburg-Landau equation with cubic nonlinearity in $1+1$ space-time dimension, with $\Gamma_1 = \mathbb{T}^2 (= S^1 \times S^1)$ – the two-torus. We

[†]IBM Research, T. J. Watson Research Center, 1101 Kitchawan Road, Route 134, Yorktown Heights, NY, 10598 USA (lopezva@us.ibm.com).

note, however, that it should be straightforward to apply the methodology described in this paper to other evolutionary parameter-dependent PDEs invariant under the action of a group of continuous transformations.

The complex Ginzburg-Landau equation (CGLE) is a widely studied PDE which has become a model problem for the study of nonlinear evolution equations exhibiting chaotic spatio-temporal dynamics, as well as being of interest in the context of pattern formation. It has applications in various fields, including fluid dynamics and superconductivity. (For details see, for example, [2, 24, 28, 40] and references therein.) Following [26], we consider here the CGLE with cubic nonlinearity in one spatial dimension,

$$\frac{\partial A}{\partial t} = RA + (1 + i\nu)\frac{\partial^2 A}{\partial x^2} - (1 + i\mu)A|A|^2, \quad (1)$$

with periodic boundary conditions

$$A(x, t) = A(x + L_x, t), \quad (2)$$

and spatial period $L_x = 2\pi$. The CGLE also appears in the literature in the form

$$\frac{\partial A}{\partial t} = A + (1 + i\nu)\frac{\partial^2 A}{\partial x^2} - (1 + i\mu)A|A|^2, \quad A(x, t) = A(x + L, t), \quad (3)$$

but note that with a change of variables $x \rightarrow (L_x/L)x$, $t \rightarrow (L_x/L)^2 t$, $A \rightarrow (L_x/L)A$ one obtains equation (1), with $R = (L/L_x)^2$. Thus we adopt the formulation (1) without loss of generality and, henceforth, when we refer to *the CGLE* we mean equation (1) with the boundary conditions (2) unless otherwise noted.

Equation (1) describes the time evolution of a complex-valued field $A(x, t)$. The parameters R , ν , and μ in the equation are real. When $R > 0$ there is, in general, nontrivial spatio-temporal behavior and this is therefore the region of interest. The parameters ν and μ are measures of the linear and nonlinear dispersion, respectively [2, 24]. In the form (1) the CGLE generates a continuous semiflow on a variety of spaces [5, 12, 24, 38].

As will be discussed in detail in Section 2, the CGLE has a three-parameter group $G = \mathbb{T}^2 \times \mathbb{R}$ of continuous symmetries generated by space-time translations and a rotation of the complex field A . Thus, we focus our study on invariant solutions of the CGLE, namely, the ones that in addition to (1) and (2) satisfy

$$A(x, t) = e^{i\varphi} A(x + S, t + T) \quad (4)$$

for some $(\varphi, S) \in \mathbb{T}^2$ and $T > 0$. The interest here is on invariant solutions of the CGLE having multiple frequencies active in their temporal spectrum, not on single-frequency solutions $A(x, t) = B(x)e^{i\omega t}$ [11, 17, 19] or generalized traveling waves $A(x, t) = \rho(x - vt)e^{i\phi(x - vt)}e^{i\omega t}$, where ρ and ϕ are real-valued functions and ω is some frequency [2, 8, 28, 39], which have

been considered more extensively than the multiple-frequency class. The CGLE is also invariant under the action of the discrete group of transformations $A(x, t) \rightarrow A(-x, t)$ and thus solutions of the CGLE may also be fixed by this \mathbb{Z}_2 -symmetry. While it is not uncommon in studies to center on solutions fixed by the \mathbb{Z}_2 -symmetry (for example, even solutions), we make no such restriction here in order to work with a broader solution space.

Since we are actually working with a 3-parameter family (1) of equations, this family defines *implicitly* a fibered space $\mathcal{S} \xrightarrow{p} \mathcal{B}$ over the space of parameters $\mathcal{B} = \{(R, \nu, \mu)\} \subset \mathbb{R}^3$, where \mathcal{S} is the total space of solutions of (1) and \mathcal{B} forms the base of the fibered space. Moreover, the group G acts on the total space of solutions \mathcal{S} . Therefore, we consider the quotient fibered space $\mathfrak{M} \xrightarrow{\pi} \mathcal{B}$ modulo this action. Here $\mathfrak{M} = \mathcal{S} / \sim$ is the total moduli space, where \sim is a relation between the points of \mathcal{S} established by the group action which is compatible with p , that is, for any $s', s \in \mathcal{S}$, $s' \sim s$ if and only if $p(s') = p(s)$ and there exists a $g \in G$ such that $s' = g \cdot s$. Then π is the map induced by p after taking the quotient, and the points of \mathfrak{M} are in one-to-one correspondence with G -orbits whose elements are all mapped by p to the same point in the base \mathcal{B} . Thus, geometrically we have a fibered space, that is, a triple $(\mathfrak{M}, \mathcal{B}, \pi)$, depicted in Figure 1, whose fibers $\mathcal{M}_{R, \nu, \mu} = \pi^{-1}(R, \nu, \mu)$ over each point $(R, \nu, \mu) \in \mathcal{B}$ of the base are moduli spaces of solutions of the CGLE. Note that we do not know the explicit form of the map π . It is defined implicitly by equation (1). In essence, our goal is to understand and reveal its properties. Therefore, the aim of the present study is to acquire a more global view of (a part of) the fibered space of G -orbits of the CGLE and its structure as we move around the point (R, ν, μ) in the base space \mathcal{B} .

More precisely, and referring again to Figure 1, here we are interested in the (sub)fibered space $(\mathcal{I}, \mathcal{B}, \pi|_{\mathcal{I}}) \subset (\mathfrak{M}, \mathcal{B}, \pi)$, where the points of the subspace $\mathcal{I} \subset \mathfrak{M}$ are G -orbits of *invariant* solutions of the CGLE. Namely, these are solutions that satisfy, in addition to (1)–(2), the functional equation (4). Then the fiber of $\pi|_{\mathcal{I}}$, $\mathcal{I}_{R, \nu, \mu} = (\pi|_{\mathcal{I}})^{-1}(R, \nu, \mu) \subset \mathcal{M}_{R, \nu, \mu}$, over each point $(R, \nu, \mu) \in \mathcal{B}$ of the base is a moduli space of such invariant solutions of the CGLE. Note that a G -orbit in $\mathcal{I}_{R, \nu, \mu}$ is determined uniquely by a quadruple $(A(x, t, R, \nu, \mu), \varphi(R, \nu, \mu), S(R, \nu, \mu), T(R, \nu, \mu))$, where $A(x, t, R, \nu, \mu)$ is an element of the orbit (that is, an invariant solution) over the point $(R, \nu, \mu) \in \mathcal{B}$. Further, for each point $(R, \nu, \mu) \in \mathcal{B}$ the space $\mathcal{I}_{R, \nu, \mu}$ is a union $\mathcal{I}_{R, \nu, \mu} = \bigcup_{\alpha} \Sigma_{R, \nu, \mu}^{(\alpha)}$ of symmetry classes $\Sigma_{R, \nu, \mu}^{(\alpha)} \subset \mathcal{I}_{R, \nu, \mu}$ of G -orbits. A number of such G -orbits and their symmetry classes were found in [26] at a particular point $(R_o, \nu_o, \mu_o) \in \mathcal{B}$. The main goal here is to understand structural changes in the spaces $\mathcal{I}_{R, \nu, \mu}$ as we trace paths in the fibered space $(\mathcal{I}, \mathcal{B}, \pi|_{\mathcal{I}})$, starting from a set of G -orbits in the fiber $\mathcal{I}_{R_o, \nu_o, \mu_o}$ and carrying them into another fiber $\mathcal{I}_{R_n, \nu_n, \mu_n}$ over a point $(R_n, \nu_n, \mu_n) \neq (R_o, \nu_o, \mu_o)$ in the base \mathcal{B} using a path following method [32].

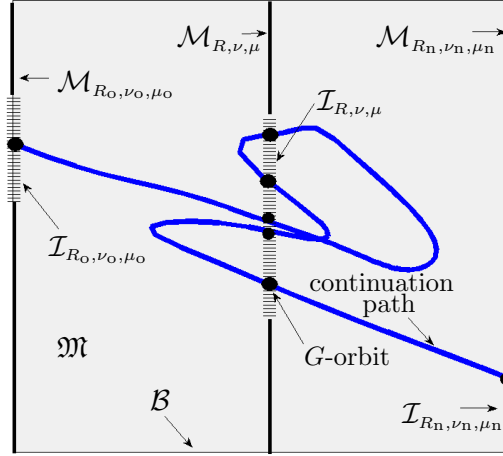


Figure 1: Fibered space $(\mathfrak{M}, \mathcal{B}, \pi)$

Indeed, structural changes associated with additional symmetry breaking or gaining (vanishing and appearance of symmetry classes in $\mathcal{I}_{R, \nu, \mu}$) were frequently uncovered in the parameter regions traversed. This includes the identification of new symmetry classes (see, for example, the metamorphosis of the moduli space along the path $\mathcal{A}^{(13)}$ – Section 4.1 and Figure 9). Thus a complex and interesting structure of the fibered space $(\mathcal{I}, \mathcal{B}, \pi|\mathcal{I})$ was revealed. Sections 2 and 4 describe in detail the additional symmetries that are being gained or broken at particular values of the CGLE parameters. Such (abrupt) structural changes amount to a kind of “phase transition” in the moduli space, which is an interesting aspect to be considered as a focus for a subsequent detailed investigation.

To put all of the above in context, in contrast to studies which are concerned with continuation (deformation) of a single critical, singular or other non-generic point (with or without symmetry) of the space of solutions of (1) (for example, solutions which are stable, steady-states, or of the aforementioned traveling waves class) and their bifurcations, ours should be viewed as a study “in the large” of properties of the 3-dimensional family of moduli spaces $\mathcal{I}_{R, \nu, \mu}$ of invariant solutions within a certain general functional class, being approximated with a spectral-Galerkin discretization (the details of which appear in Section 3.1).

As we focus on solutions of the CGLE having the invariance (4), henceforth when we refer to *G-orbits (of solutions of the CGLE)* we mean *G-orbits of invariant solutions* of the CGLE which satisfy (4), unless otherwise indicated. We also note that during the continuation, most often the final parameter region of interest was sought by moving in the direction of varying values of R . However, at times we had to venture into a subdomain

of the CGLE parameter space \mathcal{B} by moving in a direction of varying ν and μ as well. Newton’s method, which is commonly used in path following methods [1, 22], is employed to solve an underdetermined system of nonlinear algebraic equations resulting from the discretization of the CGLE. To the best of our knowledge, the way in which the Newton step is computed here is new. The approach is conceptually simple, yet that is where its value lies: it led to the efficient computation of an accurate Newton step, making the solution of a computationally challenging problem with a large number (up to 32,260) of unknowns practical without the need of a cluster or supercomputer. These and other aspects of the numerical methodology are discussed in Section 3. We note here that the Newton step used is defined from the Moore-Penrose inverse [6]. This is one technique used in numerical continuation [1, 41], without the need to define phase, or gauge, conditions [22] to augment the underdetermined system. This offers an advantage since the best (or a suitable) choice of phase conditions may be problem dependent. The question of whether to impose phase conditions, or to simply work directly with the underdetermined system, thus arises. Here we chose to explore the latter approach. However, understanding the advantages that working with phase conditions may offer over the chosen approach is important and should be considered as a follow-up investigation.

As a bi-product of our study we note that, taking the presence of positive Lyapunov exponents for typical (that is, non-invariant) solutions as an indication of chaotic dynamics [33], both the initial and final parameter regions in our study exhibit chaotic behavior. Specifically, non-invariant solutions in the initial and final parameter region have, respectively, 5 and 16 positive Lyapunov exponents.¹ This provides another motivation for conducting this study, which is to evaluate the potential benefits of using numerical continuation (on problems with a large number of unknowns) to continue multiple, distinct, unstable invariant solutions from one chaotic regime into another with the aim of ending, again, with multiple, distinct, unstable invariant solutions in the final region. One question that arises (see also [9]) is whether a significant number of the distinct solutions used as initial points to continue on will actually lead to solutions in distinct G -orbits in the final parameter region. While the possibility of this not happening cannot be ruled out, we found that options like alternating the choice of continuation parameter, or particular settings for tuning parameters in the numerical solvers, can increase the possibility of reaching a multitude of distinct G -orbits in the final desired parameter region.

A detailed account of the results obtained is provided in Section 4. We note here that the set of G -orbits in the fiber $\mathcal{I}_{R_0, \nu_0, \mu_0}$ used as starting points in the path following method

¹Lyapunov exponents for typical (non-invariant) solutions were computed using the technique from [7].

correspond to the first 15 G -orbits listed in the Appendix from [26]; these were selected simply to follow the order listed in said Appendix. The G -orbits from this initial set were carried from the point $(R_o, \nu_o, \mu_o) = (16, -7, 5)$ in the CGLE parameter space to the point $(R_n, \nu_n, \mu_n) = (100, -7, 5)$. The number of unknowns to solve for ranged between 4,000 and 32,260. Both the number of 15 G -orbits from [26] and the final point (R_n, ν_n, μ_n) in the CGLE parameter space were chosen because we deemed them to be sufficient to help us gain insight into the symmetry changes occurring in the spaces $\mathcal{I}_{R,\nu,\mu}$ of the fibered space $(\mathcal{I}, \mathcal{B}, \pi|\mathcal{I})$, as well as to allow us to evaluate the potential for success of the proposed approach for computing multiple unstable invariant solutions in fixed parameter regions of a dynamical system which exhibits chaotic behavior.

The initial set of G -orbits led to distinct, new G -orbits of invariant solutions of the CGLE along the continuation paths and in the final parameter region. The solutions in the resulting G -orbits are unstable, and have multiple modes and frequencies active in their spatial and temporal spectra, respectively. The fact that the computed solutions are unstable suggests that they may belong to the set of (infinitely many) unstable periodic orbits embedded in chaotic attractors [10, 23, 9]. This direction, by itself, is certainly very interesting to pursue in a future study of the dynamics of the CGLE.

To conclude the introduction we note that previous numerical continuation studies of the CGLE include [37], where bifurcations from a stable rotating wave to two-tori (of the generalized traveling wave class) were identified. Values of $L_x = 1$ and $R \leq 180$ in the formulation (1)–(2) were considered, giving $L \approx 13.42$ for the maximum length of the spatial period in the formulation (3). In comparison, the values $L_x = 2\pi$ and $R \leq 100$ in our study yield a maximum value of $L \approx 62.83$ in (3). The values of ν and μ used in [37] are different from those in the current study, but in both cases they belong to the Benjamin-Feir unstable region $1 + \mu\nu < 0$ [40]. A different study [8] considers traveling waves solutions, where the CGLE reduces to a system of three coupled ordinary differential equations (ODEs). Continuation was performed on the system of three ODEs for different values of L up to 512 and various chaotic regions were classified.

Other studies can be found in [30], where transition to chaos from a limit cycle of the CGLE is investigated, [20], in which the bifurcation structure and dynamics of even solutions of the CGLE are analyzed, and [25], which studies the dynamics of the CGLE in heteroclinic cycles, focused on invariant \mathbb{Z}_2 -subspaces. A numerical study on solutions fixed by the \mathbb{Z}_2 -symmetry of the CGLE and their stability with respect to symmetry-breaking perturbations appears in [3], where values of $R = 1.05, 16, 36$ are considered, and a spatial period of $L_x = 2\pi$ was used (the latter being the same as in the current study). The

subsequent study [4] considers symmetry-breaking perturbations for solutions fixed by the spatial translation symmetry, for (discrete) values of the parameter R in the range $[4.2, 80]$.

Finally, the reader may consult [1, 21, 22, 35, 41] for a background on continuation methods and software. Definitions and results concerning symmetry groups and differential equations with symmetries can be found in [15, 29, 31] and other references appearing in [26]. Although outside the scope of this paper, the interested reader is referred to [10, 23, 9] for treatments on the use of periodic orbits in the context of the study of chaotic dynamical systems, in which the computation of multiple unstable invariant solutions in fixed parameter regions is of much relevance.

2 Invariant Solutions of the CGLE and their Properties

The CGLE has a number of well known symmetries that are central to its behavior [2]. In particular, equations (1)–(2) have a three-parameter group

$$G = \mathbb{T}^2 \times \mathbb{R} \quad (5)$$

of continuous symmetries generated by space-time translations $x \rightarrow x + \sigma$, $t \rightarrow t + \tau$ and a rotation $A \rightarrow e^{i\theta} A$ of the complex field $A(x, t)$, in addition to being invariant under the action of the discrete group of transformations $A(x, t) \rightarrow A(-x, t)$ of spatial reflections. In other words, if $A(x, t)$ is a solution of equations (1)–(2), then so are

$$e^{i\theta} A(x, t), \quad (6)$$

$$A(x + \sigma, t), \quad (7)$$

$$A(x, t + \tau), \quad (8)$$

$$A(-x, t), \quad (9)$$

for any $(\theta, \sigma, \tau) \in G$. In the present study it is the group G generated by the continuous symmetries (6)–(8) which (explicitly) enters the problem formulation. Namely, for a given solution $A(x, t)$ of the CGLE, let us consider the isotropy subgroup G_A of G at A ,

$$G_A = \{(\varphi, S, T) \in G \mid A(x, t) = e^{i\varphi} A(x + S, t + T)\}, \quad (10)$$

which consists of elements of the symmetry group $G = \mathbb{T}^2 \times \mathbb{R}$ leaving A invariant. With that in mind, we pose the problem: seek solutions $A(x, t)$ of the CGLE satisfying

$$A(x, t) = e^{i\varphi} A(x + S, t + T), \quad (11)$$

for $(\varphi, S, T) \in G$ also unknown and to be determined. In other words, find orbits $G \cdot A$ of G generated by solutions A of the CGLE which are invariant under the action of some

subgroup $G_A \subset G$, that is, $G_A \cdot A = A$. Here, at least one subgroup of G_A generated by an element $(\varphi, S, T) \in G$ is also to be determined.

As is clear from (11), the case $\varphi = S = 0, T > 0$, would result in a time-periodic solution. Within the more general context of the problem of seeking solutions of a dynamical system fixed by an action of its symmetry group which also contains time translation, as is the case resulting from $T > 0$ and nonzero φ or S in (11), such invariant solutions are also referred to as *relative* time-periodic solutions. Since the solutions sought must satisfy the boundary (space-periodicity) condition (2), it is easy to see that if $S = L_x/q$ for some integer $q > 1$, then $|A(x, t)| = |A(x, t + qT)|$, whereas if both $S = L_x/q$ and $\varphi = 2\pi/q$ for some integer $q > 1$, then $A(x, t) = A(x, t + qT)$ and, therefore, $(0, 0, qT) \in G_A$ (i.e., A is time-periodic, with time period qT).

Notice that if $(\varphi, S, T) \in G_A$, the triples $(j\varphi, jS, jT)$, $j \in \mathbb{Z}$, are also elements of the isotropy subgroup G_A . Hence, (φ, S, T) generates a subgroup of G_A . Thus, the problem that we aim to solve numerically can be described succinctly as follows:

1. Given a point $p_0 = (R_0, \nu_0, \mu_0)$ in the parameter space of the CGLE, find a solution $A_{p_0}(x, t)$ of the CGLE and a generator $(\varphi(p_0), S(p_0), T(p_0))$ of a subgroup of the isotropy subgroup $G_{A_{p_0}}$, such that condition (11) holds. That is, A_{p_0} is an invariant solution of the CGLE under the action of the subgroup of $G_{A_{p_0}}$ generated by $(\varphi(p_0), S(p_0), T(p_0))$.
2. Then, starting from $p_0 = (R_0, \nu_0, \mu_0)$, vary the point $p = (R, \nu, \mu)$ along a subspace in the parameter space of the CGLE, ending at a point $p_N = (R_N, \nu_N, \mu_N)$, to find a sequence of new invariant solutions $A_p(x, t)$ and generators $(\varphi(p), S(p), T(p))$ of subgroups of their corresponding isotropy subgroups G_{A_p} .

In reference [26] we found 77 distinct unstable invariant solutions (that is, 77 G -orbits generated by distinct invariant solutions) of the CGLE at the point $p_0 = (R_0, \nu_0, \mu_0) = (16, -7, 5)$ of the parameter space of the CGLE, thus addressing the first part of the problem. Here, we take the first 15 of these solutions, per the listing from the Appendix in [26], and address the second part of the problem. Specifically, using numerical continuation (as described in Section 3) we found 15 sequences (or discrete continuation paths)

$$\begin{aligned} \mathcal{A}^{(i)} = \{ & A_{p_k^{(i)}}(x, t); (\varphi(p_k^{(i)}), S(p_k^{(i)}), T(p_k^{(i)})) \mid \\ & p_k^{(i)} = (R_k^{(i)}, \nu_k^{(i)}, \mu_k^{(i)}) \in [9, 100] \times [-7, -2.7] \times [-0.05, 5.98], \quad 0 \leq k \leq N^{(i)} \}, \end{aligned} \quad (12)$$

$i = 1, \dots, 15$, of new invariant solutions (11) of the CGLE and corresponding generators of subgroups of their isotropy subgroups $G_{A_{p_k^{(i)}}}$. In (12), the number $N^{(i)}$ of invariant solutions

in a sequence is at least 100 and, for each $i = 1, \dots, 15$, the final point $p_{N(i)}^{(i)}$ in the CGLE parameter space was fixed at $p_{N(i)}^{(i)} = (R_{N(i)}^{(i)}, \nu_{N(i)}^{(i)}, \mu_{N(i)}^{(i)}) = (100, -7, 5)$. Thus, the sequences (12) can be thought of as a deformation of an initial set of distinct G -orbits at $p_0 = (16, -7, 5)$ into a final set of G -orbits at $p_N = (100, -7, 5)$, which in this study are also distinct with the only exception being that the final orbits in the sequences $\mathcal{A}^{(2)}$ and $\mathcal{A}^{(4)}$ at p_N happened to coincide (details are provided in Section 4). In other words, if we think of the space of G -orbits as fibered over the parameter space \mathcal{B} of the CGLE (the base of the fibered space), then the sequences (or continuation paths) $\mathcal{A}^{(i)}$ can be thought of as (discrete) sections of the fibered space $(\mathcal{I}, \mathcal{B}, \pi|\mathcal{I})$. Interestingly, several of the sequences $\mathcal{A}^{(i)}$ that we have computed contain solutions with additional symmetries (which we describe in detail later in this section), thus revealing an intricate structure of the fibered space $(\mathcal{I}, \mathcal{B}, \pi|\mathcal{I})$.

Note that the meaning of the space-periodicity boundary condition (2) is that any solution $A(x, t)$ in the class of solutions of the CGLE that we seek has a subgroup in its isotropy subgroup G_A which is generated by $(0, L_x, 0)$. In other words we restrict, a priori, the class of solutions of the CGLE that we look for to the one that contains, at a minimum, solutions with symmetry (2). This allows us to represent $A(x, t)$ as a Fourier series

$$A(x, t) = \sum_{m \in \mathbb{Z}} a_m(t) e^{ik_m x}, \quad (13)$$

where $k_m = 2\pi m/L_x$ denotes the m -th wavenumber in the expansion. From the group-invariance condition (11) it then follows that the complex-valued Fourier coefficient functions $a_m(t)$ in (13) satisfy

$$a_m(t) = e^{i\varphi} e^{ik_m S} a_m(t + T) \quad (14)$$

for all $m \in \mathbb{Z}$. Because of the presence of symmetry (2), the solutions sought can be restricted to those with elements $(\varphi, S, T) \in G$ having $S \in [0, L_x)$.

Moreover, since the CGLE is invariant under the action of the group \mathbb{Z}_2 of spatial reflections $A(x, t) \rightarrow A(-x, t)$, to any solution $A(x, t)$ of the CGLE having $(0, L_x, 0)$ and (φ, S, T) as generators of subgroups of the isotropy subgroup G_A (defined in (10)) there corresponds a solution $\tilde{A}(x, t) := A(-x, t)$ having $(0, L_x, 0)$ and $(\varphi, L_x - S, T)$ as generators of subgroups of the isotropy subgroup $G_{\tilde{A}}$. This can be seen from the chain of equalities

$$\begin{aligned} \tilde{A}(x, t) &:= A(-x, t) &= e^{i\varphi} A(-x + S, t + T) &\quad \text{by (11)} \\ &= e^{i\varphi} \tilde{A}(x - S, t + T) &&\quad \text{by definition of } \tilde{A} \\ &= e^{i\varphi} \tilde{A}(x + (L_x - S), t + T) &\quad \text{by (2)}. \end{aligned} \quad (15)$$

To express the above in a more symmetric form, let us introduce $\delta = |L_x/2 - S|$. Then, if $A(x, t)$ is a solution of the CGLE having $(0, L_x, 0)$ and $(\varphi, L_x/2 \pm \delta, T)$ as generators of subgroups of the isotropy subgroup G_A , the solution $\tilde{A}(x, t) := A(-x, t)$ has $(0, L_x, 0)$ and $(\varphi, L_x/2 \mp \delta, T)$ as generators of subgroups of the isotropy subgroup $G_{\tilde{A}}$. We shall call the invariant solutions $(A; \varphi, L_x/2 \pm \delta, T)$ and $(\tilde{A}; \varphi, L_x/2 \mp \delta, T)$, as well as their corresponding orbits $G \cdot A$ and $G \cdot \tilde{A}$, *conjugate* to each other under the (involutive) action of the group \mathbb{Z}_2 of spatial reflection symmetry of the CGLE.

Now, while invariance of solutions of the CGLE other than that defined by (11) and (2) is not part of the problem formulation (10)–(11), it is clearly not excluded from it. The CGLE may admit solutions having symmetries other than (or in addition to) that defined by (11) and several of the solutions resulting from our study do have additional symmetries. In what follows we discuss some such symmetries and their properties. We emphasize that our treatment on additional types of symmetries exhibited by solutions of the CGLE is not exhaustive, but rather inclusive of material relevant to the discussion on our results in Section 4.

For instance, there may exist solutions of the CGLE satisfying

$$A(x, t) = e^{i2\pi/l} A(x + L_x/l, t), \quad \text{for some } l \in \mathbb{N}, l > 1, \quad (16)$$

$$A(x, t) = A(-x + 2c_1, t) \quad \text{for some } c_1 \in \mathbb{R}, \quad (17)$$

$$A(x, t) = -A(-x + 2c_2, t) \quad \text{for some } c_2 \in \mathbb{R}. \quad (18)$$

Note that (16) describes solutions fixed by a composition of the actions (7) and (6), and gives $(2\pi/l, L_x/l, 0)$ as one generator of a subgroup of G_A . From (16) it is also clear that the absolute value of such a solution has spatial period of L_x/l . Furthermore, by substituting condition (16) into the Fourier series expansion (13) it follows that the Fourier coefficient functions $a_m(t)$ of a solution with symmetry (16) satisfy

$$a_m(t) = \begin{cases} \text{nonzero} & \text{if } m \in \{l\tilde{m} - 1, \tilde{m} \in \mathbb{Z}\} \\ 0 & \text{otherwise.} \end{cases} \quad (19)$$

Symmetries (17) and (18) describe solutions that are, respectively, even about $x = c_1$ or odd about $x = c_2$ for some real numbers c_1, c_2 . (These solutions are fixed by a composition of the actions (9), (7), and (6).) From (17) and the periodic boundary condition (2) it follows that a solution even about $x = c_1$ is also even about $x = c_1 + L_x/2$; similarly a solution odd about $x = c_2$ is also odd about $x = c_2 + L_x/2$. The Fourier coefficient functions $a_m(t)$ in (13) of a solution even about $x = c_1$ satisfy

$$a_{-m}(t) = a_m(t) e^{ik_m 2c_1}, \quad m = 0, 1, 2, \dots, \quad (20)$$

whereas for a solution odd about $x = c_2$ one has

$$a_{-m}(t) = -a_m(t) e^{ik_m 2c_2}, \quad m = 0, 1, 2, \dots \quad (21)$$

From (19), (20), and (21) it follows that restricting the search for solutions to those possessing symmetries (16), (17), or (18) would lead to a reduction in the number of unknowns. However, as already mentioned, we did not make a priori such a restriction in order to allow for a more general set of solutions. Finally, we point out that a solution having both symmetries (16) and (17) also satisfies

$$A(-x + 2(c_1 + L_x/(2l)), t) = e^{i2\pi/l} A(x, t). \quad (22)$$

In particular, note that a solution satisfying (16) for $l = 2$ and which is even about $x = c_1$ is also odd about $x = c_2 = c_1 + L_x/4$.

For a solution satisfying (11) and (16) it follows that $(\varphi - 2\pi/l, S - L_x/l, T)$ is another generator of a subgroup of G_A . In particular, if it happens that for such a solution one has $S = L_x/l$, then $|A(x, t)| = |A(x, t + T)|$ is satisfied, whereas if both $S = L_x/l$ and $\varphi = 2\pi/l$, then $A(x, t) = A(x, t + T)$ also holds. As for invariant solutions (11) that also possess symmetry (17), note that, for each $m = 0, 1, 2, \dots$,

$$\begin{aligned} a_{-m}(t) &= e^{i\varphi} e^{-ik_m S} a_{-m}(t + T) && \text{by (14)} \\ &= e^{i\varphi} e^{-ik_m S} a_m(t + T) e^{ik_m 2c_1} && \text{by (20)}. \end{aligned} \quad (23)$$

On the other hand, for each $m = 0, 1, 2, \dots$,

$$\begin{aligned} a_{-m}(t) &= a_m(t) e^{ik_m 2c_1} && \text{by (20)} \\ &= e^{i\varphi} e^{ik_m S} a_m(t + T) e^{ik_m 2c_1} && \text{by (14)}. \end{aligned} \quad (24)$$

From (23) and (24) it follows that we must have $e^{-ik_m S} = e^{ik_m S}$ for all $m \in \mathbb{Z}$, which holds whenever S is an integer multiple of $L_x/2$ (recall that $k_m = 2\pi m/L_x$). The case for invariant solutions (11) with the additional symmetry (18) is analogous. Therefore, solutions satisfying (11) which also possess symmetries (17) or (18) exist in subspaces of the solution space $(A; \varphi, S, T)$ for which either $S = 0$ or $S = L_x/2$ (since, by the periodic boundary conditions (2), S can be restricted to be in the interval $[0, L_x)$).

To illustrate some of the aforementioned symmetries of solutions of the CGLE, Figures 2–3 display several plots that aid in visualizing the invariant properties. Figure 2 shows a solution of the CGLE having symmetry (11), but none of (16)–(18). This solution belongs to the sequence $\mathcal{A}^{(5)}$ (see (12)) resulting from the numerical continuation procedure to be described in Section 3, that is, from the continuation path for the sequence listed with id 5 in Tables 1–2. The time evolution, represented as curves on the plane with co-

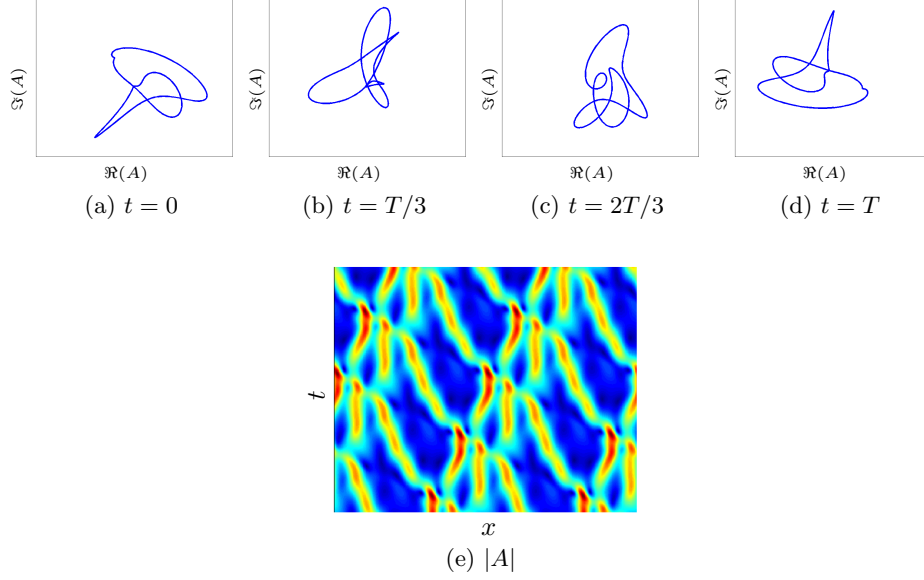


Figure 2: Solution having symmetry (11), with $T > 0$ and nonzero φ and S .

ordinates defined by the real part $\Re(A)$ and imaginary part $\Im(A)$ of the solution $A(x, t)$ at different times within the interval $[0, T]$, is depicted in Figures 2a–2d. The excitation of multiple temporal frequencies is apparent from these curves. For single-frequency solutions $A(x, t) = B(x)e^{i\omega t}$ or generalized traveling waves $A(x, t) = \rho(x - vt)e^{i\phi(x-vt)}e^{i\omega t}$ (where ω is some single frequency), plots of this kind would show, except for a rotation, the same curve at each point in time. Therefore it is clear that the solution depicted in Figures 2a–2d is not of either of these single-frequency types. Note also that the curve at time $t = T$ differs only by a rotation from that at time $t = 0$ due to the rotation of the complex field $A(x, 0) \rightarrow e^{i\varphi}A(x + S, T)$. Repeated patterns resulting from invariance due to time periodicity and the nonzero space translation S is better observed from surface plots of the absolute value $|A|$ of $A(x, t)$ over several space and time periods, as in Figure 2e.

A solution possessing all of the symmetries (16)–(18), in addition to the symmetry (11), is shown in Figure 3. The plots represent a solution which belongs to the sequence of solutions under id 15 in Tables 1–3, computed at the point $(R, \nu, \mu) = (100, -7, 5)$ of the CGLE parameter space. Surface plots of the real part $\Re(A)$, imaginary part $\Im(A)$, and absolute value $|A|$ of the solution $A(x, t)$ are shown in Figures 3a–3c, where $(x, t) \in [0, 2L_x] \times [0, 2T]$, that is, the surfaces are plotted over two space and two time periods. For this solution, symmetry (16) holds with $l = 2$. Since, in addition, the solution is even about $x = \tilde{m}L_x/4$, for $\tilde{m} \in \mathbb{Z}$ odd, it follows from (22) that the solution is also odd about

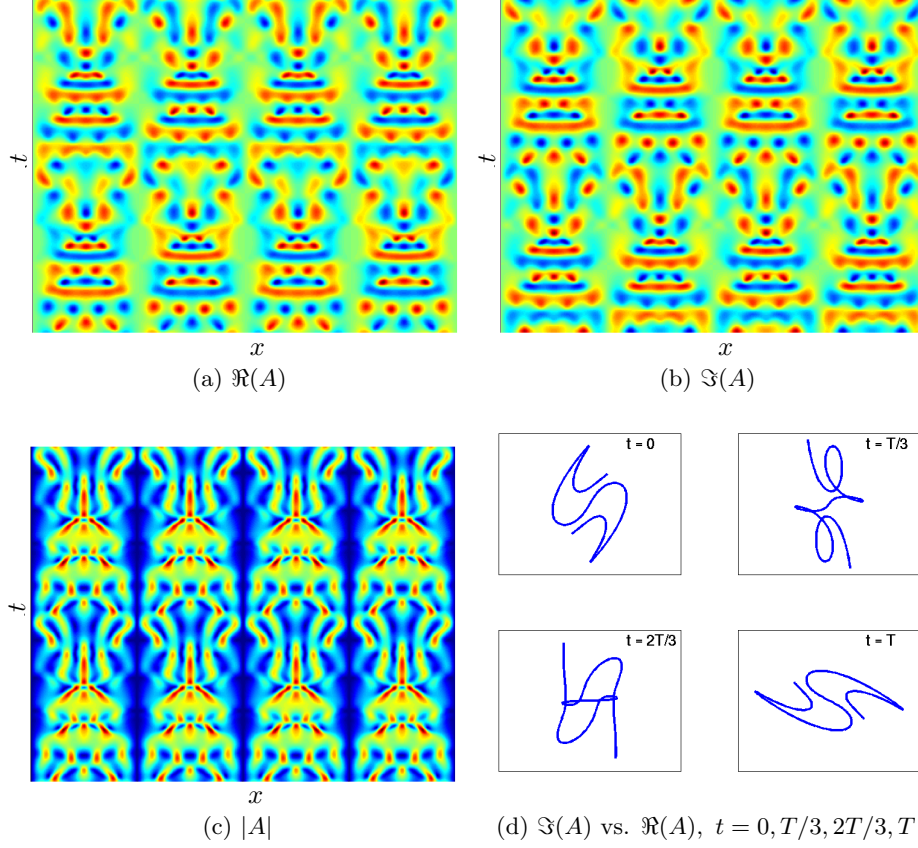


Figure 3: Solution having symmetries (16), for $l = 2$, (17), and (18), in addition to (11).

$x = (\tilde{m} + 1)L_x/4$. Finally, the absolute value of the solution has spatial period $L_x/2$ and is time-periodic, with period T . As seen in Figures 3a–3d, pattern similarities in both space and time are easily observed in the presence of the additional symmetries (16)–(18).

We conclude this section by noting the following fact. Suppose that for some $(\tilde{\varphi}, c, \tilde{T}) \in G$, where G is the group of continuous symmetries of the CGLE (refer to (5)), a solution $A(x, t)$ of the CGLE has the symmetry

$$A(x, t) = e^{i\tilde{\varphi}} A(-x + c, t + \tilde{T}). \quad (25)$$

The Fourier coefficient functions $a_m(t)$ in (13) of such a solution satisfy

$$a_{-m}(t) = a_m(t + \tilde{T}) e^{i\tilde{\varphi}} e^{ik_m c}, \quad m = 0, 1, 2, \dots \quad (26)$$

The right-hand side of (25) is the result of the (left) action on $A(x, t)$ of the composition $(\tilde{\varphi}, c, \tilde{T}) \circ (x \rightarrow -x)$, and after a (left) action of said composition on both sides of (25) one

obtains that

$$\begin{aligned} A(x, t) &= e^{i\tilde{\varphi}} A(-x + c, t + \tilde{T}) \\ &= e^{i2\tilde{\varphi}} A(x, t + 2\tilde{T}). \end{aligned} \quad (27)$$

Hence $(2\tilde{\varphi}, 0, 2\tilde{T}) \in G_A$, where G_A is the isotropy subgroup defined in (10). Also, note that we have

$$[(\tilde{\varphi}, c, \tilde{T}) \circ (x \rightarrow -x)]^2 = (2\tilde{\varphi}, 0, 2\tilde{T}) \in G,$$

for any element $(\tilde{\varphi}, c, \tilde{T})$ in the group G of continuous symmetries of the CGLE. Conversely, let $(\tilde{\varphi}, 0, \tilde{T}) \in G_A$ for some solution $A(x, t)$ of the CGLE. Then we have

$$[(\tilde{\varphi}/2 + k\pi, c, \tilde{T}/2) \circ (x \rightarrow -x)]^2 = (\tilde{\varphi}, 0, \tilde{T})$$

for every $k \in \mathbb{Z}$ and $c \in \mathbb{R}$. Therefore, solutions of the CGLE with symmetry (25) do possess symmetry (11) of the type we seek, and, conversely, a solution with symmetry (11) may also possess the additional symmetry (25). An example of solutions having both symmetries (11) and (25) is described in Section 4 (cf. Figure 9). Such solutions appeared in the continuation path for the sequence listed with id 13 in Tables 1–3, that is, in the sequence $\mathcal{A}^{(13)}$ (see (12)).

Finally, note that if a solution $A(x, t)$ of the CGLE having symmetry (11) for $S = 0$ or $S = L_x/2$ also satisfies

$$A(x, t) = e^{i\hat{\varphi}} A(-x + \hat{c}, t) \quad (28)$$

for some real numbers $\hat{\varphi}$ and \hat{c} (an example being solutions with the additional symmetry (17), where $\hat{\varphi} = 0$, or with the additional symmetry (18), for which $\hat{\varphi} = \pi$), then

$$A(x, t) = e^{i(\hat{\varphi} + 2\varphi)} A(-x + \hat{c}, t + 2T).$$

That is, such solution A also has symmetry (25). Therefore, one should expect to find solutions having both symmetries (11) and (25) in subspaces of the space of solutions $(A; \varphi, S, T)$ for which either $S = 0$, by (27), or $S \in \{0, L_x/2\}$, if symmetry (28) is also present.

3 Numerical Method

As noted in Section 1, having computed previously in [26] a set of unstable invariant solutions of the CGLE for fixed values of the parameters (R, ν, μ) , our first goal is to employ numerical continuation to carry solutions of this initial set into solutions in a regime

with a different set of parameter values (R, ν, μ) . To achieve this, we discretize using Fourier series expansions in both space and time to derive an underdetermined system of nonlinear algebraic equations from which invariant solutions of the CGLE are sought. This discretization was used in the previous study [26]. The associated material which is directly relevant to the current study is summarized in Sections 3.1 and 3.2 below in order to make the present account self-contained. Details concerning the numerical continuation, which was not a component of the previous study [26], are provided in Section 3.3.

3.1 Derivation of Nonlinear Algebraic Equations

Since the boundary conditions (2) are periodic in x , we use the spatial Fourier series (13) and substitute into the CGLE (1) to obtain an infinite system of ordinary differential equations (ODEs),

$$\frac{da_m}{dt} = Ra_m - k_m^2(1 + i\nu)a_m - (1 + i\mu) \sum_{m_1+m_2-m_3=m} a_{m_1}a_{m_2}a_{m_3}^*, \quad (29)$$

for the complex-valued functions $a_m(t)$. Under this transformation the symmetries (6)–(9) of equations (1)–(2) become symmetries of (29). Thus, if $\mathbf{a}(t) = (a_m(t))$ is a solution of the system of ODEs (29), then so are

$$(e^{i\theta}a_m(t)), \quad (30)$$

$$(e^{im\sigma}a_m(t)), \quad (31)$$

$$(a_m(t + \tau)), \quad (32)$$

$$(a_{-m}(t)), \quad (33)$$

for any $(\theta, \sigma, \tau) \in \mathbb{T}^2 \times \mathbb{R}$. In particular, (30) and (31) say that the ODEs (29) are invariant under the \mathbb{T}^2 -action

$$(\theta, \sigma) \cdot (a_m(t)) = (e^{i\theta}e^{im\sigma}a_m(t)).$$

We employ a spectral-Galerkin projection obtained by fixing an even number N_x and truncating the expansion (13) to include only the terms with indices m satisfying $-N_x/2 + 1 \leq m \leq N_x/2 - 1$. We then work with the corresponding finite system of ODEs which results from (29) after the Galerkin projection. Much accumulated theory and computation shows that for sufficiently large N_x the behavior of this truncation captures the essential features of the dynamics of (1)–(2) [12, 18].

From the condition (11) defining an invariant solution of the CGLE, it follows that the

corresponding solution $\mathbf{a}(t)$ of the system of ODEs (29) satisfies

$$a_m(t) = e^{i\varphi} e^{ik_m S} a_m(t+T) \quad (34)$$

for all m and t (and where φ, S, T are to be determined). It is easy to see that the set of functions

$$a_m(t) = e^{-i\frac{\varphi}{T}t} e^{-ik_m \frac{S}{T}t} \sum_{n \in \mathbb{Z}} \hat{a}_{m,n} e^{i\omega_n t}, \quad (35)$$

where $\omega_n = 2\pi n/T$ denotes the n -th frequency in the expansion, are a solution of the system of functional equations (34). Hence, they provide an appropriate representation for invariant solutions of the system of ODEs (29). Substituting (35) into the truncated system of ODEs (29) and using again a Galerkin projection obtained by fixing an even number N_t , so that the summation index in (35) runs over the range $-N_t/2 + 1 \leq n \leq N_t/2 - 1$, results in a system of nonlinear algebraic equations,

$$\mathbf{F}(\hat{\mathbf{a}}, \varphi, S, T) = \mathbf{F}_L(\hat{\mathbf{a}}, \varphi, S, T) + \mathbf{F}_{NL}(\hat{\mathbf{a}}) = \mathbf{0}, \quad (36)$$

for the complex Fourier coefficients $\{\hat{a}_{m,n}\}$ and elements (φ, S, T) of the isotropy subgroup (10). In (36), $\hat{\mathbf{a}}$ denotes a vector with components given by the coefficients $\{\hat{a}_{m,n}\}$ and the vectors $\mathbf{F}_L(\hat{\mathbf{a}}, \varphi, S, T)$ and $\mathbf{F}_{NL}(\hat{\mathbf{a}})$ are defined as

$$\mathbf{F}_L(\hat{\mathbf{a}}, \varphi, S, T) \equiv \left\{ i \left(\frac{2\pi n}{T} - \frac{\varphi}{T} - k_m \frac{S}{T} \right) \hat{a}_{m,n} - R \hat{a}_{m,n} + k_m^2 (1 + i\nu) \hat{a}_{m,n} \right\}, \quad (37)$$

and

$$\mathbf{F}_{NL}(\hat{\mathbf{a}}) \equiv \left\{ (1 + i\mu) \sum_{m_1+m_2-m_3=m} \left(\sum_{n_1+n_2-n_3=n} \hat{a}_{m_1,n_1} \hat{a}_{m_2,n_2} \hat{a}_{m_3,n_3}^* \right) \right\}. \quad (38)$$

Note that the components of the vector \mathbf{F}_L in (37) correspond to the discretization of the linear terms in the CGLE and those of \mathbf{F}_{NL} in (38) to that of the nonlinear term $(1 + i\mu)A|A|^2$. Furthermore, in defining the vector $\hat{\mathbf{a}}$ (and similarly for \mathbf{F}_L and \mathbf{F}_{NL}) we are implicitly assigning an ordering on the coefficients $\{\hat{a}_{m,n}\}$ that uniquely determines an indexing for the components of $\hat{\mathbf{a}}$. Henceforth, such a convention should be understood whenever applicable. Finally, we will use the notation in (36) to denote both the system of complex equations and the system obtained by splitting (36) into its real and imaginary parts, as it should be clear from the context which case applies.

Splitting the equations into their real and imaginary parts, one has that (36) is an underdetermined system of $2(N_x - 1)(N_t - 1)$ real equations in $2(N_x - 1)(N_t - 1) + 3$ real unknowns. Solutions of this system of equations will give the desired invariant solutions of the truncated system of ODEs via the expansion (35). We note here that with the

introduction of the representation (35), the symmetry group $G = \mathbb{T}^2 \times \mathbb{R}$ of (1) and (29) descends to the symmetry group $\mathbb{T}^3 = \mathbb{T}^2 \times \mathbb{S}^1$ of (36), acting on the space $(\{\hat{a}_{m,n}\}, \varphi, S, T)$ of solutions of (36). Henceforth, by a slight abuse of notation, we refer to both symmetry groups $\mathbb{T}^2 \times \mathbb{R}$ and \mathbb{T}^3 as G .

The symmetries (30)–(33) of the ODEs (29) induce symmetries of the system of algebraic equations (36). Note that if $(\{\hat{a}_{m,n}\}, \varphi, S, T)$ solves $\mathbf{F} = \mathbf{0}$, then for any $(\theta, \sigma, \tau) \in \mathbb{T}^3$

$$(\{e^{i\theta} \hat{a}_{m,n}\}, \varphi, S, T), \quad (39)$$

$$(\{e^{im\sigma} \hat{a}_{m,n}\}, \varphi, S, T), \quad (40)$$

$$(\{e^{in\tau} \hat{a}_{m,n}\}, \varphi, S, T), \quad (41)$$

$$(\{\hat{a}_{-m,n}\}, \varphi, -S, T), \quad (42)$$

are also solutions. From the continuous symmetries (39)–(41), it follows that the set of solutions of $\mathbf{F} = \mathbf{0}$ splits into orbits $\mathcal{O}_{(\hat{\mathbf{a}}, \varphi, S, T)}$ of the symmetry group \mathbb{T}^3 ,

$$\mathcal{O}_{(\hat{\mathbf{a}}, \varphi, S, T)} := \{(\theta, \sigma, \tau) \cdot (\hat{\mathbf{a}}, \varphi, S, T) \mid (\theta, \sigma, \tau) \in \mathbb{T}^3\}, \quad (43)$$

where the action of \mathbb{T}^3 on a point $(\hat{\mathbf{a}}, \varphi, S, T)$ is defined by

$$(\theta, \sigma, \tau) \cdot (\hat{\mathbf{a}}, \varphi, S, T) = (\{e^{i\theta} e^{im\sigma} e^{in\tau} \hat{a}_{m,n}\}, \varphi, S, T). \quad (44)$$

That is, \mathbb{T}^3 acts on $\hat{\mathbf{a}}$ via multiplication by the matrix $\text{diag}(e^{i\theta} e^{im\sigma} e^{in\tau})$, and it acts trivially on (φ, S, T) . Finally we note that, for the system of nonlinear algebraic equations (36), the transformation (42) induced by (9) maps a solution

$$(\{\hat{a}_{m,n}\}, \varphi, L_x/2 \pm \delta, T) \quad (45)$$

of (36) to another (conjugate) solution

$$(\{\hat{a}_{-m, n+m}\}, \varphi, L_x/2 \mp \delta, T) \quad (46)$$

of (36), where, again, $\delta = |L_x/2 - S|$. (Refer to the paragraph containing (15).)

3.2 Jacobian Matrix

The Jacobian matrix of the system $\mathbf{F} = \mathbf{0}$ of nonlinear algebraic equations (36) is dense so, as the number of unknowns (and equations) increases, it becomes unfeasible to solve linear systems with the Jacobian as coefficient matrix using direct methods. However, matrix-vector products with the Jacobian matrix of \mathbf{F} can be computed efficiently for the problem at hand, making the use of iterative methods for solving linear systems a viable option. We proceed to review the calculation of this matrix-vector product since it is an essential feature of the Newton step computation employed in the numerical continuation.

Let $J_{\hat{\mathbf{a}}}$ denote the matrix whose columns correspond to derivatives of \mathbf{F} with respect to the real and imaginary parts of the unknowns $\{\hat{a}_{m,n}\}$, and let $\hat{\mathbf{v}}$ be a vector with components given by the coefficients in the truncated Fourier series expansion of a function $V(x, t)$. Assume that $J_{\hat{\mathbf{a}}}$ is evaluated at a given point $(\hat{\mathbf{a}}, \varphi, S, T)$. The product $J_{\hat{\mathbf{a}}} \hat{\mathbf{v}}$ can then be computed as²

$$J_{\hat{\mathbf{a}}} \hat{\mathbf{v}} = \mathbf{DF}_L(\hat{\mathbf{v}}, \varphi, S, T) + \mathbf{DF}_{NL}(\hat{\mathbf{a}}, \hat{\mathbf{v}}), \quad (47)$$

where $\mathbf{DF}_L(\hat{\mathbf{v}}, \varphi, S, T) \equiv \mathbf{F}_L(\hat{\mathbf{v}}, \varphi, S, T)$ (as defined in (37)) and $\mathbf{DF}_{NL}(\hat{\mathbf{a}}, \hat{\mathbf{v}})$ is a vector with components given by the coefficients in the truncated Fourier series expansion (in both space and time) of $(1 + i\mu)(A^2 V^* + 2|A|^2 V)$. This matrix-vector product operation follows from the discretization (analogous to that used for the CGLE) of the first variational derivative of equation (1),

$$\frac{\partial V}{\partial t} = RV + (1 + i\nu) \frac{\partial^2 V}{\partial x^2} - (1 + i\mu)(A^2 V^* + 2|A|^2 V).$$

Furthermore, as can be seen from system (36)–(38), the operation of computing a matrix-vector product with the columns of the Jacobian matrix of \mathbf{F} corresponding to the derivatives with respect to φ , S , and T poses no difficulty.

It follows then that matrix-vector products with the Jacobian matrix of \mathbf{F} can be easily computed without the need of explicitly calculating the (full) Jacobian. Note also from (37) that the portion of the Jacobian matrix coming from the discretized linear terms $\mathbf{F}_L(\hat{\mathbf{a}}, \varphi, S, T)$ in the CGLE is a block diagonal matrix, with 2×2 blocks, whose components are easily computed. Hence, solving linear systems with this block diagonal matrix poses no complications. This is advantageous since this block diagonal matrix provides an effective preconditioner for some of the matrix-free iterative methods when solving linear systems having the Jacobian as coefficient matrix for the problem at hand. (Refer to Section 3.3.)

Finally, we note that the matrix $J_{\hat{\mathbf{a}}}$ (refer to (47)), whose columns correspond to derivatives of \mathbf{F} with respect to the real and imaginary parts of the unknowns $\{\hat{a}_{m,n}\}$, is singular at a solution $(\hat{\mathbf{a}}, \varphi, S, T)$ of $\mathbf{F} = \mathbf{0}$. This is relevant for the computation of the Newton step, discussed in Appendix A. The vectors in the null space of $J_{\hat{\mathbf{a}}}$ result from a basis for the space of infinitesimal generators of the action (44) of \mathbb{T}^3 on the point $(\hat{\mathbf{a}}, \varphi, S, T)$. The reader may consult [26] for further details.

²Note that in the right-hand side of (47) we are actually using $\hat{\mathbf{v}}$ to denote a vector with the *complex* numbers $\{\hat{v}_{m,n}\}$ as components, whereas in the left-hand side of (47) $\hat{\mathbf{v}}$ denotes a vector with *real* components that are the real and imaginary parts of the coefficients $\{\hat{v}_{m,n}\}$. We make use of this slight abuse of notation in this paper since the intended meaning should be clear from the context.

3.3 Numerical Continuation of Solutions

The numerical continuation was done using the Library of Continuation Algorithms (LOCA) software package [35], specifically with the aid of the algorithms provided to track steady state solutions of discretized PDEs as a function of a single parameter. The option of pseudo arc length continuation was used in order to allow for turning points [1] to be followed. Although we are not computing steady state solutions in this study, it is clear that the feature of tracking steady state solutions in the LOCA package provides the capability of solving a system of nonlinear algebraic equations using numerical continuation (which is what we need). We thus take advantage of this feature, particularly to handle the step size control, that is, the changes in the continuation parameter, including that in the vicinity of turning points, at each continuation step. For specific details on the implementation of said capabilities in the LOCA software, the reader is referred to the documentation [35]. Associated details on input information required from the user appear in Section 4.2, where comments on aspects related to the numerical simulations are provided.

Newton’s method is used to solve the system of nonlinear algebraic equations in the numerical continuation, and the user must supply the LOCA package with a routine for computing the Newton step. That is, the user must provide a routine that solves a linear system having as coefficient matrix the Jacobian of the system of nonlinear algebraic equations. For this purpose, we employed iterative methods for solving linear systems, specifically the GMRES solver from the Meschach software package [36]. The computation of the nonlinear terms \mathbf{F}_{NL} in (36) and $\mathbf{D}\mathbf{F}_{\text{NL}}$ in (47), needed, respectively, for the evaluation of \mathbf{F} and that of the product of the Jacobian matrix and a vector, was done using the FFTW software package [13]. For further efficiency in the calculations we used POSIX threads (pthreads) programming [27] in our routines, taking thus advantage of the multiple cores available nowadays in personal workstations.

Rather than augmenting the system (36) with an additional set of equations in order to work with an equal number of equations and unknowns [26], we work with the underdetermined system (36) and consider here a Newton step defined from the Moore-Penrose inverse [6]. This yields a minimum norm solution of the system of linear equations with the underdetermined Jacobian as coefficient matrix, and is one approach used in numerical continuation methods [1, 41]. A detailed description of the computation of the Newton step for the present study appears in Appendix A. We note that the use of conceptually simple techniques led to an accurate and efficient computation of the Newton step. The techniques employed made it practical to solve a computationally challenging problem without the need of a cluster or supercomputer.

4 Numerical Study and Results

The procedure described in Section 3 was applied to a subset of the unstable invariant solutions of the CGLE computed at the point $(R, \nu, \mu) = (16, -7, 5)$ of the CGLE parameter space (without employing continuation) in the preceding study [26], in order to carry them into solutions in a regime with an increased value of the parameter R , namely to the region at the point $(R, \nu, \mu) = (100, -7, 5)$ of the CGLE parameter space. As indicated in Section 1, chaotic behavior is exhibited both at the initial and final parameter regions.

A summary of the obtained results is gathered in Tables 1–3 and Figure 4b. Already from them, we see that our probe into the moduli space of G -orbits reveals a complicated and interesting structure. To start with, along each of the continuation paths $\mathcal{A}^{(i)}$, $i = 1, \dots, 15$, we were able to compute a number $N^{(i)}$ (listed in Table 2) of new distinct G -orbits of solutions of the CGLE (each one of which corresponds to a distinct invariant solution of the CGLE). Thus, the continuation paths $\mathcal{A}^{(i)}$, $i = 1, \dots, 15$, can be thought of as (discrete) sections of the fibered space of G -orbits over the space of parameters of the CGLE.

Before describing the content of Tables 1–3, let us list the possibilities that may occur when numerically continuing a set of distinct G -orbits. (These are analogous to the cases listed later in Section 4.1 where we examine continuation paths which revisit a fiber over a point in the CGLE parameter space after a series of steps while performing continuation for a single G -orbit.) Suppose that $A_{p_0}^{(i)} \in \mathcal{A}^{(i)}$ and $A_{p_0}^{(j)} \in \mathcal{A}^{(j)}$, $i \neq j$, are two invariant solutions representing distinct G -orbits at the initial point $p_0^{(i)} = p_0^{(j)} = (R_0, \nu_0, \mu_0)$ in the CGLE parameter space, where $\mathcal{A}^{(i)}$ and $\mathcal{A}^{(j)}$ are, respectively, the continuation paths (12) emanating from each one of the two initial invariant solutions. Given two points $p_k^{(i)}$ and $p_l^{(j)}$ in the CGLE parameter space and two invariant solutions $A_{p_k}^{(i)} \in \mathcal{A}^{(i)}$ and $A_{p_l}^{(j)} \in \mathcal{A}^{(j)}$, it may happen that $p_k^{(i)} = p_l^{(j)}$, and we have to consider several possibilities. Namely, whether the invariant solutions $A_{p_k}^{(i)}$ and $A_{p_l}^{(j)}$ represent (i) the same G -orbit, that is, $(\varphi(p_k^{(i)}), S(p_k^{(i)}), T(p_k^{(i)})) = (\varphi(p_l^{(j)}), S(p_l^{(j)}), T(p_l^{(j)}))$ and there exists some $(\theta, \sigma, \tau) \in G$ such that $A_{p_k}^{(i)} = (\theta, \sigma, \tau) \cdot A_{p_l}^{(j)}$; (ii) different, but conjugate, G -orbits, as defined in Section 2 (see also (45)–(46)); or (iii) different, non-conjugate, G -orbits.

After a careful analysis of all computed solutions we found that there were solutions $A_{p_k}^{(2)} \in \mathcal{A}^{(2)}$ and $A_{p_l}^{(4)} \in \mathcal{A}^{(4)}$ which represent the same G -orbit, at points $p_k^{(2)} = p_l^{(4)}$ in the range $(R, \nu, \mu) \in ([16.5, 54.4] \cup [54.7, 100]) \times [-7] \times [5]$ of CGLE parameter values. Furthermore, there were (a) solutions $A_{p_k}^{(11)} \in \mathcal{A}^{(11)}$ and $A_{p_l}^{(14)} \in \mathcal{A}^{(14)}$ which represent the same G -orbit, at points $p_k^{(11)} = p_l^{(14)}$ in the range $(R, \nu, \mu) \in [11.5, 60] \times [-7] \times [5]$; (b) solutions $A_{p_k}^{(11)} \in \mathcal{A}^{(11)}$, $A_{p_l}^{(14)} \in \mathcal{A}^{(14)}$, and $A_{p_j}^{(15)} \in \mathcal{A}^{(15)}$ which represent the same

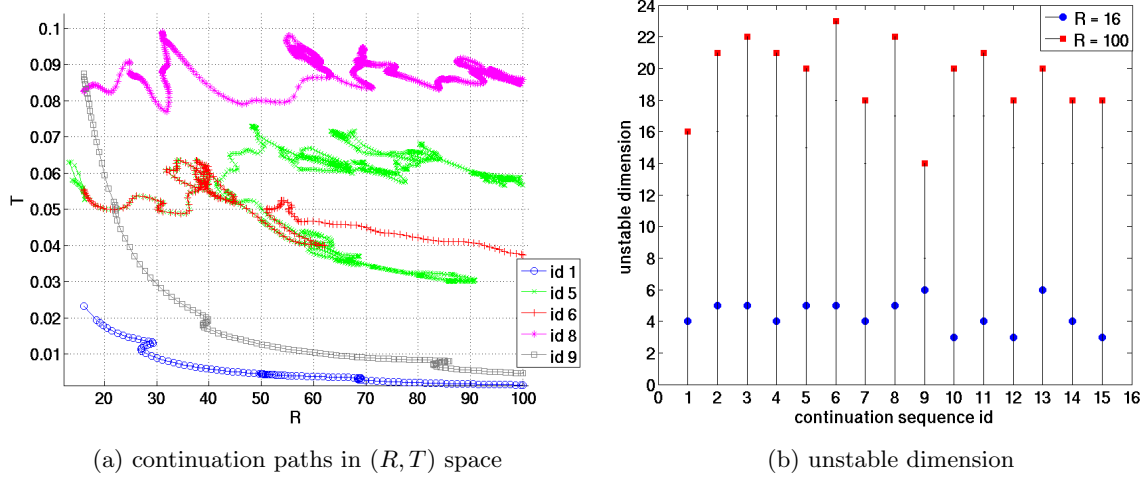


Figure 4: (a) Representative continuation paths, depicted by plotting the time period T as a function of the parameter R . (b) Unstable dimension of solutions at the initial and final parameter regions for each sequence $\mathcal{A}^{(i)}$, $i = 1, \dots, 15$.

G -orbit, at points $p_k^{(11)} = p_i^{(14)} = p_j^{(15)}$ in the range $(R, \nu, \mu) \in [16, 60] \times [-7] \times [5]$; (c) solutions $A_{p_i^{(14)}} \in \mathcal{A}^{(14)}$ and $A_{p_j^{(15)}} \in \mathcal{A}^{(15)}$ which represent the same G -orbit, at points $p_i^{(14)} = p_j^{(15)}$ in the range $(R, \nu, \mu) \in [16, 85] \times [-7] \times [5]$; and (d) solutions $A_{p_k^{(5)}} \in \mathcal{A}^{(5)}$ and $A_{p_l^{(6)}} \in \mathcal{A}^{(6)}$ which represent conjugate G -orbits, at points $p_k^{(5)} = p_l^{(6)}$ in the range $(R, \nu, \mu) \in [17, 59.5] \times [-7] \times [5]$. The latter case is illustrated in Figure 4a, where the graphs in (R, T) -space for the sequences $\mathcal{A}^{(5)}$ and $\mathcal{A}^{(6)}$ overlap for the aforementioned range of R . Therefore, multiple representatives of same G -orbits were carefully accounted for and only one of them was taken as representative of the corresponding distinct G -orbit.

Figure 4a illustrates as well that, while for the sequences $\mathcal{A}^{(1)}$ and $\mathcal{A}^{(9)}$, for example, the numerical continuation progressed in a relatively smooth manner, such was not the case in general. Turning points and overlapping paths, exemplified by the depiction of the graphs $T = T(R)$ for sequences $\mathcal{A}^{(5)}$, $\mathcal{A}^{(6)}$, and $\mathcal{A}^{(8)}$ in Figure 4a, were frequently encountered. These features revealed intricate and challenging parameter regions for traversal. (Details appear in Section 4.1 below.)

Table 1 lists the values of (φ, S, T) for the solutions at the starting CGLE parameter values of $(R, \nu, \mu) = (16, -7, 5)$ and at the final values of $(R, \nu, \mu) = (100, -7, 5)$, as well the unstable dimension³ and spatial period of the invariant solutions at the aforementioned parameter values. Per the third column in Table 1, the listed solutions are unstable. As

³The unstable dimension of an invariant (or relative time-periodic) solution is the number of eigenvalues of the associated relative monodromy matrix having magnitude greater than one; see [26].

id	$(\varphi, S, T)_{(R, \nu, \mu)=(16, -7, 5)} \rightarrow (\varphi, S, T)_{(R, \nu, \mu)=(100, -7, 5)}$	unstable dimension	spatial period
1	(5.3622, 3.8544, 0.0233) \rightarrow (5.9158, 3.8856, 0.0015)	4 \rightarrow 16	$L_x \rightarrow L_x$
2	(2.8849, 3.0956, 0.0539) \rightarrow (0.1088, 3.1416, 0.0130)	5 \rightarrow 21	$L_x \rightarrow L_x/3$
3	(0.0011, 3.9709, 0.0539) \rightarrow (5.5905, 2.2876, 0.0193)	5 \rightarrow 22	$L_x \rightarrow L_x$
4	(2.9343, 3.1416, 0.0540) \rightarrow (0.1088, 3.1416, 0.0130)	4 \rightarrow 21	$L_x \rightarrow L_x/3$
5	(4.6093, 1.4537, 0.0547) \rightarrow (0.9483, 1.0333, 0.0567)	5 \rightarrow 20	$L_x \rightarrow L_x$
6	(4.5165, 4.7061, 0.0556) \rightarrow (5.2620, 5.1417, 0.0374)	5 \rightarrow 23	$L_x \rightarrow L_x$
7	(0.2436, 2.3887, 0.0608) \rightarrow (4.0066, 3.1416, 0.0319)	4 \rightarrow 18	$L_x \rightarrow L_x$
8	(4.7959, 3.0824, 0.0825) \rightarrow (3.8358, 3.4537, 0.0859)	5 \rightarrow 22	$L_x \rightarrow L_x$
9	(0.2876, 2.4431, 0.0875) \rightarrow (0.3410, 1.3964, 0.0047)	6 \rightarrow 14	$L_x \rightarrow L_x$
10	(5.0251, 3.1416, 0.0895) \rightarrow (5.3410, 3.1728, 0.0491)	3 \rightarrow 20	$L_x \rightarrow L_x$
11	(2.6023, 3.1719, 0.1046) \rightarrow (1.5060, 3.2037, 0.0762)	4 \rightarrow 21	$L_x \rightarrow L_x$
12	(2.6575, 3.1209, 0.1078) \rightarrow (4.5024, 2.4768, 0.0754)	3 \rightarrow 18	$L_x \rightarrow L_x$
13	(6.0553, 0.0032, 0.1106) \rightarrow (2.5186, 0.0000, 0.0803)	6 \rightarrow 20	$L_x \rightarrow L_x$
14	(2.6063, 3.1057, 0.1128) \rightarrow (4.0182, 3.2164, 0.0948)	4 \rightarrow 18	$L_x \rightarrow L_x$
15	(2.2500, 3.1416, 0.1146) \rightarrow (1.7332, 3.1416, 0.1020)	3 \rightarrow 18	$L_x \rightarrow L_x$

Table 1: Properties of solutions at initial and final points of continuation.

seen from Table 1 and the depiction in Figure 4b, the solutions used as initial points for the numerical continuation have unstable dimension ranging between 3 and 6, whereas the new solutions in the final parameter region have unstable dimension between 14 and 23. The time period for the initial solutions is in the range $T \in (0.02, 0.12)$ (or $T \in (0.32, 1.92)$ for the formulation (3) of the CGLE); for the new solutions in the final parameter region we have $T \in (0.001, 0.11)$ (or $T \in (0.1, 11)$ for the formulation (3) of the CGLE). No truly time-periodic solutions were identified (although their existence in the regions traversed is not ruled out), as all solutions have a nonzero value for the rotation angle φ .

Except for the sequence $\mathcal{A}^{(1)}$, listed with id 1 in Tables 1–2, for which the solution at the final parameter values has only a few temporal frequencies active and appears to be close to a single-frequency solution, all of the solutions have broad spatial and temporal spectra. Also, aside from the sequences $\mathcal{A}^{(2)}$ and $\mathcal{A}^{(4)}$, listed, respectively, with ids 2 and 4 in Tables 1–3, all of the resulting solutions retained the same spatial period of length L_x as that of the starting solutions. The spatial period $L_x/3$ of solutions in the sequences $\mathcal{A}^{(2)}$ and $\mathcal{A}^{(4)}$ was acquired (for both sequences) at parameter values $(R, \nu, \mu) \approx (20.2, -7, 5)$. The ending solutions in these two sequences are different elements of the same orbit (43) of the symmetry group G at the final point in parameter space, although the corresponding starting solutions belong to different orbits. As for the other sequences, the solutions at the final point in parameter space belong to different orbits of the symmetry group G .

Breaking or gaining of the additional symmetries (17) or (18) was often detected, and gain of the additional symmetries (16) and (25) was also uncovered. (More details appear in Tables 2–3 and Section 4.1.) We did not observe a change in stability of the solutions at

id	additional symmetries			continuation on R only	$N^{(i)}$
	start of continuation	in between	end of continuation		
1	none	none	none	yes	112
2	none	(17)	(17)	yes	188
3	(16), $l = 2$	(16), $l = 2$	(16), $l = 2$	no	179
4	(17)	(17)	(17)	yes	233
5	none	none	none	yes	634
6	none	none	none	yes	191
7	none	(16), $l = 2$, (17), (18)	(16), $l = 2$, (17), (18)	no	179
8	none	(17)	none	yes	489
9	(16), $l = 3$	(16), $l = 3$	(16), $l = 3$	yes	116
10	(17)	(17)	none	no	385
11	none	(16), $l = 2$, (17), (18)	(16), $l = 2$	yes	415
12	none	none	none	no	472
13	none	(25)	(25)	no	526
14	none	(16), $l = 2$, (17), (18)	(16), $l = 2$	yes	615
15	(16), $l = 2$, (17), (18)	(16), $l = 2$, (17), (18)	(16), $l = 2$, (17), (18)	yes	438

Table 2: Additional symmetries associated to G -orbits along the continuation paths.

the points where additional symmetries were gained or broken, but the unstable dimension would usually change at said points (with an increase or decrease of 1 or 2). Table 2 indicates which additional symmetries, if any, the invariant solutions possess, whether continuation was done only on the parameter R or not (as will be discussed in Section 4.1), as well as the number $N^{(i)}$ of distinct CGLE parameter points for which solutions were found in each sequence $\mathcal{A}^{(i)}$, $i = 1, \dots, 15$ (see (12)). To determine the number $N^{(i)}$, we counted two points in the resulting numerical continuation path of the sequence $\mathcal{A}^{(i)}$, say $p_j^{(i)} = (R_j^{(i)}, \nu_j^{(i)}, \mu_j^{(i)})$ and $p_k^{(i)} = (R_k^{(i)}, \nu_k^{(i)}, \mu_k^{(i)})$, where $j \neq k$, as distinct if $\|p_j^{(i)} - p_k^{(i)}\|_2 \geq 0.05$. Approximate values of the CGLE parameters (R, ν, μ) at which any additional symmetry was gained or broken during the numerical continuation are listed in Table 3, only for those sequences where symmetry gaining or breaking behavior occurred.

4.1 Features from the Solution Process

Recall that we start the continuation from a point (G -orbit) in the fiber over the initial point $(R, \nu, \mu) = (16, -7, 5)$ in the base (space of parameters) tracing a path of G -orbits (invariant solutions) which belong to fibers of the moduli space over the moving point in the base. (This was done 15 times starting from 15 different points (G -orbits) in the moduli space belonging to the fiber over the initial point $(R, \nu, \mu) = (16, -7, 5)$ in the base.) Given the nature of the continuation method used and its implementation, one may revisit a fiber

id	approximate (R, ν, μ) values: type of symmetry gained/broken
2	$(16.5, -7, 5)$: (17) gained \rightarrow $(20.6, -7, 5)$: (17) broken \rightarrow $(53.4, -7, 5)$: (17) gained
4	$(20.6, -7, 5)$: (17) broken \rightarrow $(54.7, -7, 5)$: (17) gained
7	$(100, -7, 0.3)$: (16), $l = 2$, gained \rightarrow $(100, -7, -0.02)$: (17), (18) gained
8	$(32.6, -7, 5)$: (17) gained \rightarrow $(85.5, -7, 5)$: (17) broken
10	$(82.8, -7, 5.97)$: (17) broken \rightarrow $(82.9, -7, 5.97)$: (17) gained \rightarrow $(85.5, -7, 5.97)$: (17) broken
11	$(12.17, -7, 5)$: (16), $l = 2$, (17), (18) gained \rightarrow $(60.1, -7, 5)$: (17), (18) broken
13	$(16, -5.6, 3.4)$: (25) gained
14	$(16.2, -7, 5)$: (17) gained \rightarrow $(15.8, -7, 5)$: (16), $l = 2$, (18) gained \rightarrow $(80.6, -7, 5)$: (17), (18) broken \rightarrow $(80.8, -7, 5)$: (17), (18) gained \rightarrow $(78.7, -7, 5)$: (17), (18) broken
15	$(72.5, -7, 5)$: (17), (18) broken \rightarrow $(71.2, -7, 5)$: (17), (18) gained \rightarrow $(84.8, -7, 5)$: (17), (18) broken \rightarrow $(67.7, -7, 5)$: (17), (18) gained \rightarrow $(80.9, -7, 5)$: (17), (18) broken \rightarrow $(84.9, -7, 5)$: (17), (18) gained

Table 3: Summary of symmetries gained/broken along the continuation paths.

over a particular point (R, ν, μ) in the base several times during the continuation process. In other words, a continuation path in the moduli space of G -orbits may turn around.

To give an idea of the performance of the methodology employed, Figures 5–7 show several plots corresponding to application of the procedure for the sequence $\mathcal{A}^{(8)}$ (see (12)), listed with id 8 in Tables 1–3. Continuation in this case was done on the CGLE parameter R only. Paths resulting from the continuation appear in Figure 5. Specifically, Figures 5a, 5b, and 5c depict the resulting continuation paths by displaying, respectively, the values of the time period T , space translation S , and rotation⁴ φ as functions of the continuation parameter R . Note from Figure 5b that within the range of $R \approx 32.6$ through $R \approx 85.5$ the value of S remained constant. The start of this interval of constant S corresponds to a step in the continuation process at which the resulting solution gained the additional symmetry (17); this symmetry was broken at the point in the path where S ceases to be constant. (Recall that solutions with symmetries (11) and (17) exist in subspaces of the solution space $(A; \varphi, S, T)$ for which either $S = 0$ or $S = L_x/2$; see Section 2.)

The depictions in Figure 5 make it convenient to identify turning points in the continuation path and, for a given (fixed) value of the continuation parameter, whether there may

⁴Since it was not strictly necessary, the constraint $\varphi \in [0, 2\pi)$ was not explicitly enforced when solving the system of nonlinear algebraic equations (36). Furthermore, after performing a series of preliminary test runs, we found no advantage (from a computational point of view) in enforcing it. The values of φ in Figure 5c are displayed as they resulted from the solution of the system (36), and should be taken modulo an integer multiple of 2π , mapping them back to the interval $[0, 2\pi)$.

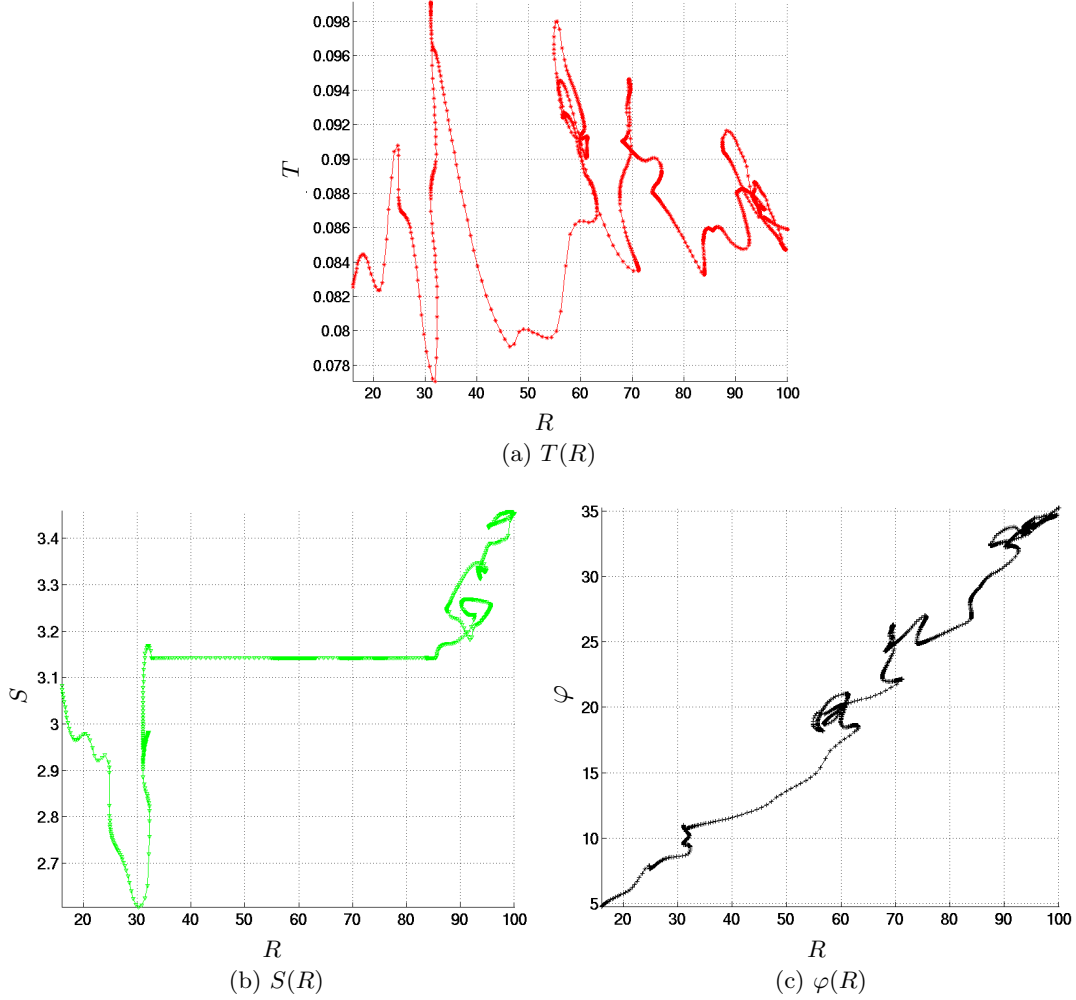


Figure 5: Continuation sequence $\mathcal{A}^{(8)}$: Paths traversed by T , S , and φ , as functions of R .

exist multiple solutions of $\mathbf{F} = \mathbf{0}$ in the path. For example, in Figure 5a one can identify four points where the line $R = 90$ intersects the curve $T(R)$. These four points correspond to four invariant solutions computed at the same particular point (R, ν, μ) in parameter space. Then, the multitude of solutions associated with this point in parameter space can be inspected to determine whether they are different elements of the same orbit (43) of the symmetry group G , whether they belong to conjugate orbits of the symmetry group, or whether they belong to different (non-conjugate) orbits of the symmetry group.

Spectra for several solutions in the path from $R = 16$ to $R = 100$ are shown in Figure 6. As expected, an increase in the value of R requires more terms in the expansions (13) and (35) in order to keep a suitable decay in both the spatial and temporal spectra for the

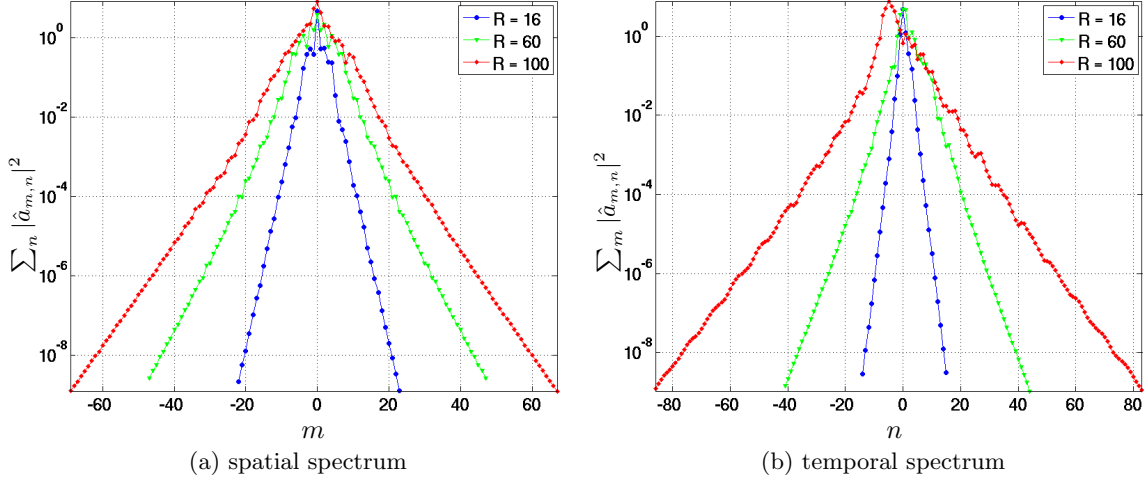


Figure 6: Spectra for three solutions in the sequence $\mathcal{A}^{(8)}$, at values of $R = 16, 60, 100$ ($\nu = -7$, $\mu = 5$).

solutions. Finally, surface plots of the real part $\Re(A)$, imaginary part $\Im(A)$, and absolute value $|A|$ for the solutions whose spectra are shown in Figure 6 appear in Figure 7, where the aforementioned gain and, thereafter, loss of symmetry (17) can be observed.

The example above illustrates the general situation that one faces. By this we mean that, due to the use of the arc-length continuation option from the LOCA package [35], which was the appropriate choice for us because it allows for turning points in the path following process, it is possible (i.e., inherent in the continuation algorithm) that a point $p_l = (R_l, \nu_l, \mu_l)$ in the CGLE parameter space may return to itself, that is, $p_{k+l} = p_l$, after k continuation steps. In such a situation, we must consider different cases for the solutions $(A_{p_{k+l}}; \varphi(p_{k+l}), S(p_{k+l}), T(p_{k+l}))$ and $(A_{p_l}; \varphi(p_l), S(p_l), T(p_l))$. Namely, whether said solutions represent (i) the same G -orbit, that is, $(\varphi(p_{k+l}), S(p_{k+l}), T(p_{k+l})) = (\varphi(p_l), S(p_l), T(p_l))$ and there exists some $(\theta, \sigma, \tau) \in G$ such that $A_{p_{k+l}} = (\theta, \sigma, \tau) \cdot A_{p_l}$; (ii) different, but conjugate, G -orbits, as defined in Section 2 (see also (45)–(46)); or (iii) different, non-conjugate, G -orbits. Along a continuation path, say $\mathcal{A}^{(i)}$, many returns to a same point $p_l^{(i)}$ do occur. However, we include only one of the invariant solutions computed at $p_l^{(i)}$ in the count $N^{(i)}$ in Table 2, since the presentation of the complete analysis of the multitude of invariant solutions that were computed at such “revisited” points is out of the scope of this paper.

Challenging behavior that arose during the numerical continuation was often due to traversal of values of the continuation parameter in a cyclic manner, specifically related to the cases (i) and (ii) listed in the previous paragraph. As a result, the continuation path within these cycles would contain (different) elements in the same G -orbit, or solutions

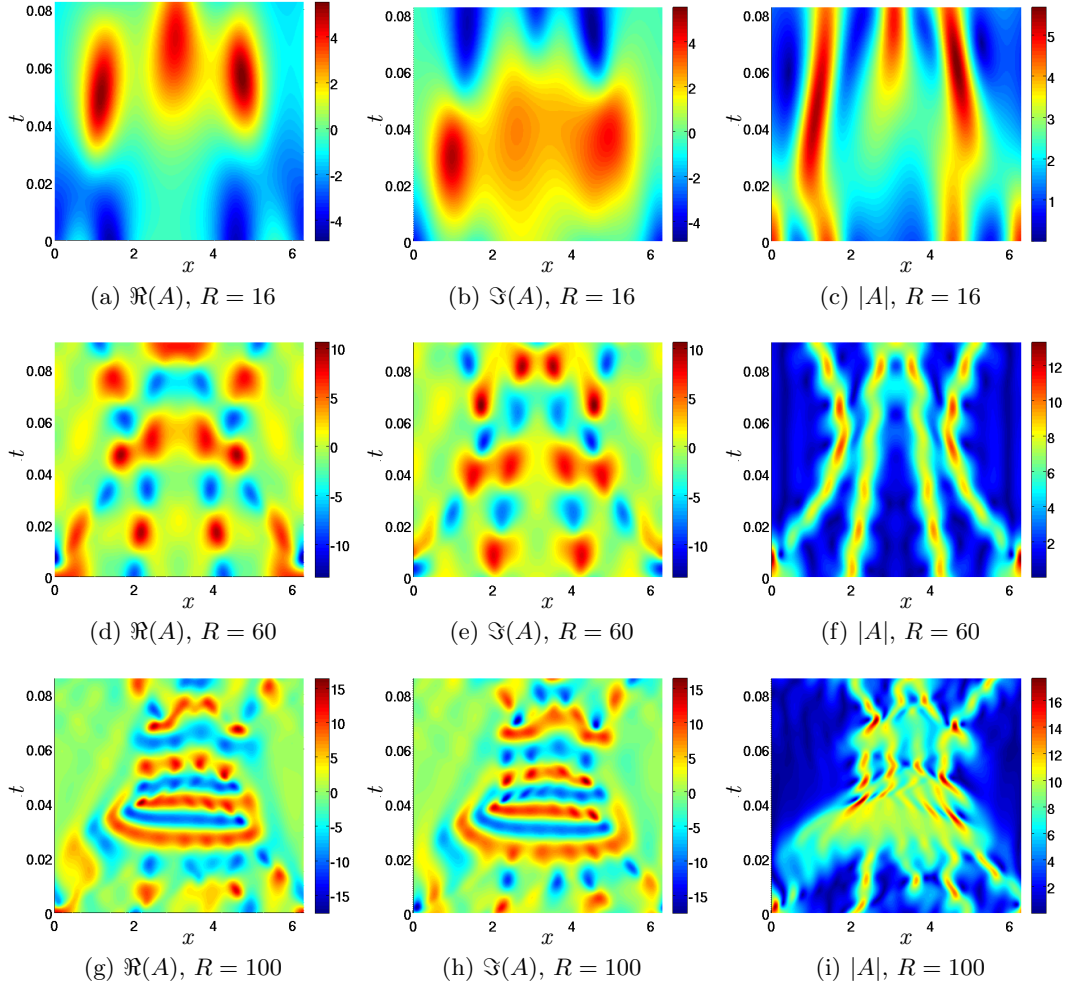


Figure 7: Surface plots of the real part $\Re(A)$, imaginary part $\Im(A)$, and absolute value $|A|$ for three solutions in sequence $\mathcal{A}^{(8)}$, at values of $\nu = -7, \mu = 5$ and $R = 16$ (top), $R = 60$ (middle), and $R = 100$ (bottom). Symmetry (17) was gained at $(R, \nu, \mu) \approx (32.6, -7, 5)$ and broken at $(R, \nu, \mu) \approx (85.5, -7, 5)$. Hence A is even (about $x = \pi$) for $R = 60$, but not for $R = 16, 100$. [Click here](#) for a movie depicting the continuation path in (φ, S, T) space, as well as solutions represented by plotting $\Im(A(x, 0))$ vs. $\Re(A(x, 0))$ at a sequence of continuation steps.

representing conjugate G -orbits (cf. (15) and (45)–(46)). Within the cycles, solutions at the turning points in the continuation path were in the vicinity of solutions with additional symmetries, or near solutions with a smaller spatial period L_x/q_1 for some integer $q_1 > 1$ or smaller time period T/q_2 for some integer $q_2 > 1$. Often the LOCA continuation algorithm [35] would exit from the cycles automatically, so that the procedure would again start yielding solutions in different, non-conjugate, G -orbits, as well as continue to make progress towards the goal of reaching the (desired) final point in the CGLE parameter

space. However, sometimes the continuation algorithm would get caught in said cycles. We discuss instances of these scenarios in the following paragraphs.

An example of such cyclic behavior is depicted in Figure 8 for the sequence $\mathcal{A}^{(11)}$, listed with id 11 in Tables 1–3. Continuation was done on the parameter R only. Figure 8a displays the values of the continuation parameter R , time period T , space translation S , and rotation φ as functions of the continuation step number. Traversal of repeated values for R , T , S , and φ is observed from the sub-figures in Figure 8a, where it is also seen that the cycling behavior stops when $R \approx 12.17$, at around continuation step number 180 (where S becomes constant), at which point the additional symmetries (16)–(18) are gained.

Looking at Figure 8b, where the value of the space translation S is plotted as a function of the continuation parameter R , one can see the cyclic behavior of R resulting in a symmetric curve with respect to the horizontal line at the vertical axis value of $L_x/2 = \pi$. The path depicted in Figure 8b, represented by the curve $S(R)$, contains conjugate solutions (cf. (15) and (45)–(46)). More precisely, the numerical continuation path for values of $R \in [12, 20]$ that contains conjugate solutions is the one that yields the symmetric curve about the horizontal line at the value of $L_x/2 = \pi$ (seen in Figure 8b). That is, points on the curve $S(R)$ that are mirror images with respect to the line $L_x/2 = \pi$ correspond to conjugate solutions under the spatial reflection symmetry of the CGLE, which belong to conjugate orbits of the symmetry group G . The additional symmetry (17) was gained at a value of $R \approx 12.17$, and at this point the cycling behavior stops and the spatial translation S takes on the value of $L_x/2$, as solutions with symmetries (11) and (17) exist in subspaces of the solution space $(A; \varphi, S, T)$ for which either $S = 0$ or $S = L_x/2$ (refer to Section 2).

Also, the additional symmetry (16), for $l = 2$, was gained along with the additional symmetry (17). Recall from (19) that the Fourier coefficients $\{\hat{a}_{m,n}\}$ of solutions with symmetry (16), for $l = 2$, satisfy $\hat{a}_{m,n} = 0$ if m is even. Thus, we can visualize gain of this additional symmetry by selecting a coefficient $\hat{a}_{m,n}$, for some even m and some n , and plotting its value as a function of the continuation parameter R , as done in Figure 8c for the coefficient $\hat{a}_{0,0}$. At the point when this additional symmetry is gained, for $R \approx 12.17$, we see that the real part of the coefficient $\hat{a}_{0,0}$ goes from (around) 0.22 to 0, whereas its imaginary part goes from (around) 0.1 to 0. Upon gaining the additional symmetry (16), for $l = 2$, the coefficient $\hat{a}_{0,0}$ remains equal to zero, as seen in the path depicted in Figure 8c. Finally, from (19), a solution with symmetry (16), for $l = 2$, will have nonzero Fourier coefficients $\{\hat{a}_{m,n}\}$ for odd m . This is depicted for the coefficient $\hat{a}_{-1,0}$, plotted as a function of the continuation parameter R , in Figure 8d. As seen, the coefficient $\hat{a}_{-1,0}$ remains nonzero after the additional symmetry (16) is gained (at the same time when the cycling behavior stops)

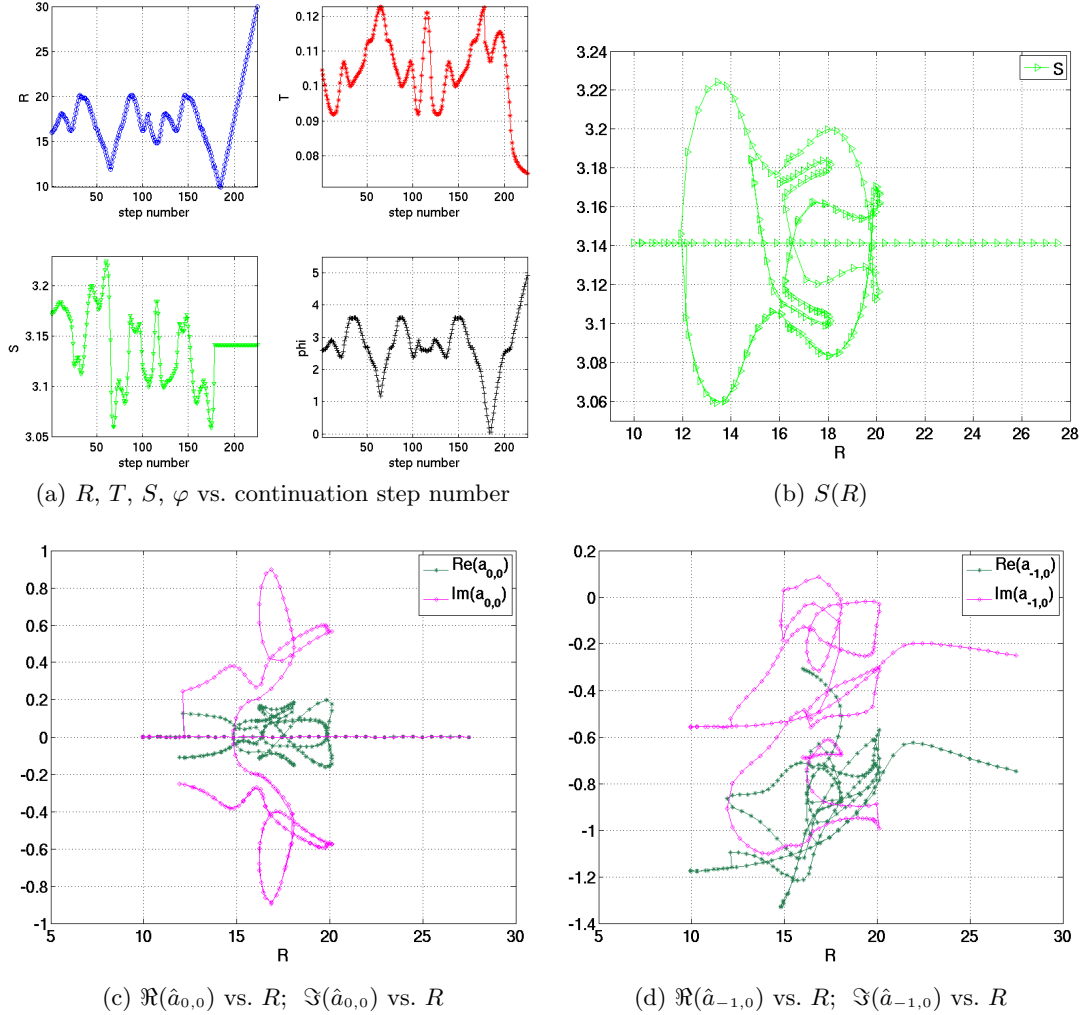


Figure 8: Cycling behavior during the numerical continuation for sequence $\mathcal{A}^{(11)}$: (a) Values of the continuation parameter R and computed generator (φ, S, T) as functions of the continuation step number. (b) S as a function of R . (c) $\Re(\hat{a}_{0,0})$ and $\Im(\hat{a}_{0,0})$ as functions of R . (d) $\Re(\hat{a}_{-1,0})$ and $\Im(\hat{a}_{-1,0})$ as functions of R . [Click here](#) for a movie depicting the continuation path in (φ, S, T) space, as well as solutions represented by plotting $\Im(A(x, 0))$ vs. $\Re(A(x, 0))$ at a sequence of continuation steps. The cycle in sub-figure (b) above can be seen during the initial steps of the path in (φ, S, T) space. Symmetries (16)–(18) were gained at $(R, \nu, \mu) \approx (12.17, -7, 5)$; symmetries (17)–(18) were broken at $(R, \nu, \mu) \approx (60.1, -7, 5)$.

at a value of $R \approx 12.17$.

The aforementioned traversal of values of the continuation parameter in a cyclic manner was quite common, and often the LOCA continuation algorithm [35] would exit from the cycles automatically, that is, without us having to stop and restart the continuation with different values for the allowed increments on the continuation parameter. Nevertheless, as an alternative for circumventing such cycling behavior, we also experimented with taking

the other parameters μ or ν in the CGLE (1) as continuation parameters. The continuation was always done on a single parameter at a time, while still all solutions were numerically continued from the regime with parameter values $(R, \nu, \mu) = (16, -7, 5)$ to the regime for $(R, \nu, \mu) = (100, -7, 5)$. As a starting point for performing continuation on an alternate parameter, we would select a solution within the cycle for which the spectra (spatial or temporal, as appropriate) did not display characteristics typical of that of solutions around the turning points in the cycle. As an example, with the solutions represented via (35), given an integer $q_1 > 1$, the Fourier coefficients $\{\hat{a}_{m,n}\}$ of a solution with spatial period L_x/q_1 have a recognizable pattern of zeros, namely, $\hat{a}_{m,n} = 0$ if m is not divisible by q_1 . So if the numerical continuation was caught in a cycle where solutions around a turning point were close to a solution with spatial period L_x/q_1 , as a starting point for performing continuation on an alternate parameter we could select a solution within the cycle for which $\sum_n |\hat{a}_{m,n}|^2 > \varepsilon$, for $m = 0, \pm 1, \dots, \pm q_1$, and some cutoff, say, $\varepsilon = 10^{-2}$.

One particular case in which it was beneficial to alternate the continuation parameter was for the sequence $\mathcal{A}^{(13)}$, for which exiting automatically from cycling behavior in the vicinity of a solution that was even and had space period $L_x/3$ and time period of $T/2$ was challenging. Hence we experimented with alternating the continuation parameter, as indicated in the previous paragraph. The continuation then led to a solution with the additional symmetry (25), along with the invariance (11). This additional symmetry was gained at parameter values of $R = 16, \nu \approx -5.6, \mu \approx 3.4$. Patterns resulting from the additional symmetry (25) can be visualized from the surface plot shown in Figure 9.

4.2 Comments on Numerical Aspects

Values of $N_x \in [48, 128]$ and $N_t \in [48, 128]$ were used, respectively, in the truncation of the spatial Fourier series expansion (13) and the representation (35). (For comparison, values of $N_x = 32$ and $N_t = 48, 64$ were used in the preceding study [26].) The number of terms N_x, N_t in each expansion was chosen so that the solutions had a decay of at least 10^{-6} in their spatial and temporal spectra. The resulting number of unknowns for the system $\mathbf{F} = \mathbf{0}$ of nonlinear algebraic equations (36) ranged between 4,000 and 32,260.

To solve the linear systems $J_s \tilde{z}_k = \tilde{b}_k$ using the GMRES iterative solver from the Meschach library [36], we set a tolerance of 10^{-9} for the residual $\|J_s \tilde{z}_k - \tilde{b}_k\|_2$ and a maximum of 3,000 GMRES iterations. Recall that the solution of said linear systems is needed for the computation of the Newton step, as described in Section 3.3 and the associated Appendix A. The number of iterations taken by the GMRES solver to meet the specified residual tolerance ranged between 90 and 2,700. In terms of actual computing time (on a

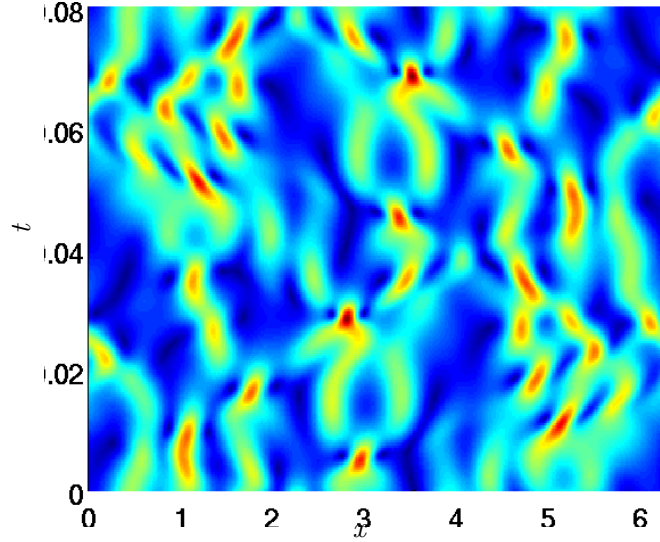


Figure 9: Surface plot of the absolute value $|A|$ for a solution in sequence $\mathcal{A}^{(13)}$, at parameter values $(R, \nu, \mu) = (100, -7, 5)$. The plot is over the space period $[0, L_x]$ on the horizontal axis and time period $[0, T]$ on the vertical axis. The solution has the additional symmetry (25), with $c = L_x$, $\hat{\varphi} = \varphi/2 + \pi$, $\hat{T} = T/2$, so $|A(x, t)| = |A(L_x - x, t + T/2)|$, as observed from the plot. [Click here](#) for a movie depicting the continuation path in (φ, S, T) space, as well as surface plots of $|A|$ at a sequence of continuation steps. The additional symmetry (25) was gained at $(R, \nu, \mu) \approx (16, -5.6, 3.4)$.

ThinkPad W530 personal workstation with 2.70 GHz processor speed), this translated to fractions of a second on the lower end to around 45-60 seconds on the higher end for the total time taken to compute the Newton step. Occasionally the maximum number of GMRES iterations was reached, in which case the computation of the Newton step was reported as failed to the main numerical continuation routine. However, in most cases convergence to the desired residual tolerance was reached with under 2,000 GMRES iterations. Solution of the system of nonlinear algebraic equations typically took 2–6 iterations for Newton’s method (a maximum of 10 Newton iterations was set). Upon convergence of Newton’s method, the residual $\|\mathbf{F}\|_2$ was on the order of 10^{-7} or less.

As for the LOCA numerical continuation library [35], recall from Section 3.3 that we performed single-parameter continuation using the option of arc-length continuation in order to allow for turning points in the path following process. Input information required by the LOCA library was set based on behavior observed for some initial runs as well as on recommendations provided in the documentation [35]. In particular, we experimented with providing the LOCA library values in the range $[-0.1, 1.0]$ for the initial change in the continuation parameter and $[0.5, 2.0]$ for the maximum increment in the continuation parameter. We found that it was best to set the initial change in the continuation parameter to be in the range $[0.01, 0.05]$, and to allow a maximum increment in the range $[0.5, 1.0]$.

Although larger values could also perform satisfactorily, in general we found that it was best for our problem to keep somewhat tight control on these increments in the sense that the number of failed attempts was then minimal (often zero). In addition, allowing large increments led several of the solutions to a single-frequency solution in the range $R \in [9, 10]$ of values of the continuation parameter. With tighter bounds on the allowed increments, the numerical continuation led to a larger variety of solutions, as discussed at the beginning of Section 4 and in Section 4.1.

Upon reaching a solution of $\mathbf{F} = \mathbf{0}$ at the final CGLE parameter values, the values of N_x and N_t in the truncated expansions (13) and (35) were increased to confirm that, with the increased number of terms in the expansions, Newton's method would converge to the same solution. (That is, to confirm that the solution of $\mathbf{F} = \mathbf{0}$ was numerically well defined.) In addition, the solution was validated against time integration of the truncated system of ODEs (29). Finally, we note that the computations were performed on a Thinkpad W530 personal workstation with 16 GB memory, four cores, with two threads per core, and 2.70 GHz processor speed. Per the discussion in Section 3.3 and the corresponding Appendix A, four threads were used concurrently when solving for the Newton step.

5 Summary and Concluding Remarks

We have considered the problem of numerical computation and deformation of invariant solutions of evolutionary partial differential equations (PDEs) with continuous symmetries. We worked in particular with the complex Ginzburg-Landau equation (CGLE)

$$\frac{\partial A}{\partial t} = RA + (1 + i\nu)\frac{\partial^2 A}{\partial x^2} - (1 + i\mu)A|A|^2$$

in 1+1 space-time dimension with periodic boundary conditions in space, which has a three-parameter group G of continuous symmetries generated by space-time translations $x \rightarrow x + \sigma$, $t \rightarrow t + \tau$ and a rotation $A \rightarrow e^{i\theta}A$ of the complex field A , and is also invariant under the action of the discrete group of transformations $A(x, t) \rightarrow A(-x, t)$ of spatial reflections. It should be straightforward to apply the methodology used to other evolutionary parameter-dependent PDEs invariant under the action of a group of continuous transformations.

The desired solutions were sought from those of an underdetermined system of nonlinear algebraic equations resulting from the use of a spectral-Galerkin discretization of the CGLE in both space and time. Given a set of previously computed G -orbits of unstable invariant solutions of the CGLE for fixed values of the parameters R , ν , and μ [26], we employed

numerical continuation to carry G -orbits of this initial set into G -orbits of invariant solutions in a regime obtained by increasing the value of R . That is, we considered the use of a path following method to solve the system of nonlinear algebraic equations, with the initial guesses for the nonlinear equations solver (Newton’s method) provided by a set of G -orbits of solutions from [26]. The CGLE exhibits chaotic behavior both at the initial and final parameter regions.

The set of initial G -orbits of (unstable) solutions led to distinct, new G -orbits of invariant solutions of the CGLE in the final (and intermediate) parameter region(s). The solutions in the resulting G -orbits are unstable, and have multiple modes and frequencies active in their spatial and temporal spectra, respectively. Thus this work and resulting solutions are an addition to the more extensively studied single-frequency and generalized traveling waves solutions of the CGLE. Symmetry gaining and breaking behavior, associated mainly with the spatial reflection symmetry $A(x, t) \rightarrow A(-x, t)$ of the CGLE, was detected frequently in the parameter regions traversed. This phenomenon is tantamount to occurrence of “phase transitions” in the space of G -orbits of solutions of the CGLE at particular values of the parameters (R, ν, μ) , and is one interesting aspect to consider as a focus for a subsequent detailed investigation.

As discussed in Section 3.3, the use of conceptually simple, but effective techniques, led to an efficient computation of the Newton step. Employing POSIX threads (pthreads) programming [27] allowed us to take advantage of the multiple cores available nowadays in personal workstations and made the solution of a computationally challenging problem with a large number of unknowns (up to 32,260 unknowns in the present study) practical without the need of a cluster or supercomputer. Freely available software, specifically the Library of Continuation Algorithms (LOCA) package [35], the Meschach library [36] for solving systems of linear algebraic equations, and the FFTW library [13] for computing fast Fourier transforms, were used as tools in the implementation of the software required to carry out the numerical continuation.

Among aspects for further consideration we mention research on techniques that may help in minimizing or circumventing excessive traversal of parameter values in a cyclic manner, per the discussion in Section 4.1. This could include alternative techniques for control of the step size in the continuation parameter or the use of multi-parameter continuation. A comparison with alternatives to the use of the Moore-Penrose inverse for computing the Newton step, specifically the use of phase or gauge conditions [22], should be also performed. Such additional features will provide a more versatile setting in which to explore further larger parameter regions (with an increasing number of unknowns and/or higher

space dimension), and enhance the understanding of the structure of the solution space of the CGLE, and in particular, the structure of the space of orbits of its symmetry group. In addition, the fact that the resulting solutions are unstable suggests that the solutions may belong to the set of (infinitely many) unstable periodic orbits embedded in chaotic attractors [10, 23, 9]. This direction, by itself, is certainly very interesting to pursue in further studies of the dynamics of the CGLE, and on the potential use of such periodic orbits in the study of chaotic dynamical systems [10, 23, 9].

Acknowledgements

The author thanks Ognyan Stoyanov for useful discussions on the topic of symmetry groups of differential equations and helpful feedback on a preliminary version of this paper, as well as for much help with installation of the Fedora operating system prior to setting up and performing the computations described here.

A Appendix: Newton Step Computation

We work with the underdetermined system of nonlinear algebraic equations (36) and consider a Newton step defined from the Moore-Penrose inverse [6]. This yields a minimum norm solution of the system of linear equations with the underdetermined Jacobian of (36) as coefficient matrix, and is one technique used in numerical continuation methods [1, 41]. However, instead of computing the desired Newton step directly from the linear system having the underdetermined Jacobian as coefficient matrix, we premultiply the linear system with a matrix composed of a subset of the columns of the Jacobian so that a numerical solution for the problem at hand may be obtained in a more efficient manner. The approach is conceptually simple, yet that is where its value lies: it allowed us to compute an accurate Newton step quickly and efficiently and made the solution of a computationally challenging problem with a large number of unknowns practical without the need of a cluster or supercomputer. The details are explained next.

Let J be a $p \times q$ matrix, $p < q$, and assume J has rank p . Let b be a vector of size $q \times 1$. Recall that the minimum norm solution z of the system of linear equations

$$Jz = b \tag{48}$$

given by the Moore-Penrose inverse is [1]

$$z = J^T(JJ^T)^{-1}b. \tag{49}$$

Computing the solution z from (49) thus requires the solution of a linear system having JJ^T as coefficient matrix.⁵ As is well known, the numerical solution of a system of linear algebraic equations may be obtained using a variety of methods, either direct [14] or iterative ones [16]. A main distinction between these two classes of methods is that the use of direct methods requires explicitly the availability of the coefficient matrix, whereas for iterative methods what is needed is the ability to perform matrix-vector products with the coefficient matrix. Hence, iterative methods are an attractive option when explicit computation of the coefficient matrix is not feasible or is inconvenient, and multiplication of the coefficient matrix and a vector can be performed (efficiently) without explicit computation of the coefficient matrix. As discussed in Section 3.2, the latter applies to the problem at hand. Therefore we considered the use of iterative methods, in particular the generalized minimal residual (GMRES) method [16, 34] due to its robustness and suitability for non-symmetric systems. Since the matrix JJ^T in (49) is symmetric we also explored the possibility of using the conjugate gradient (CG) method for symmetric systems [16], but, as will be discussed below, the GMRES method is a more suitable option for our problem.

The convergence behavior of iterative methods for solving linear systems is dependent on the method as well as on various other factors, for example, certain properties of the coefficient matrix or the problem from which the linear system is derived. In the case of the GMRES method, one desirable property for fast convergence is for the eigenvalues of the coefficient matrix to be clustered around a few values, away from zero [16]. Another important issue is that the use of iterative methods for solving linear systems typically requires the use of a preconditioner in order to perform efficiently. Generally speaking, preconditioning refers to multiplying the linear system (on the left or right) by a matrix such that the resulting system has the properties needed for optimal or enhanced performance of the particular method under consideration (and yields a solution for the unpreconditioned (i.e., original) linear system). For thorough treatments on iterative methods for solving linear systems, the interested reader is referred to [16] and references therein. Here we restrict ourselves to a brief discussion on the behavior resulting from the use of the GMRES and CG methods for the problem at hand.

Figure 10 depicts the typical convergence behavior exhibited by the GMRES and CG methods when used to compute the solution of systems of linear equations having as coefficient matrix the Jacobian of the system (36) of nonlinear algebraic equations, after splitting the equations into their real and imaginary parts. In the figure, J denotes the underde-

⁵The components of the Jacobian matrix in our computations are real, hence our use of the terms *transpose* and *symmetric* when referring to the matrix J in the discussion that follows, instead of the more general terms *conjugate transpose* and *Hermitian*.

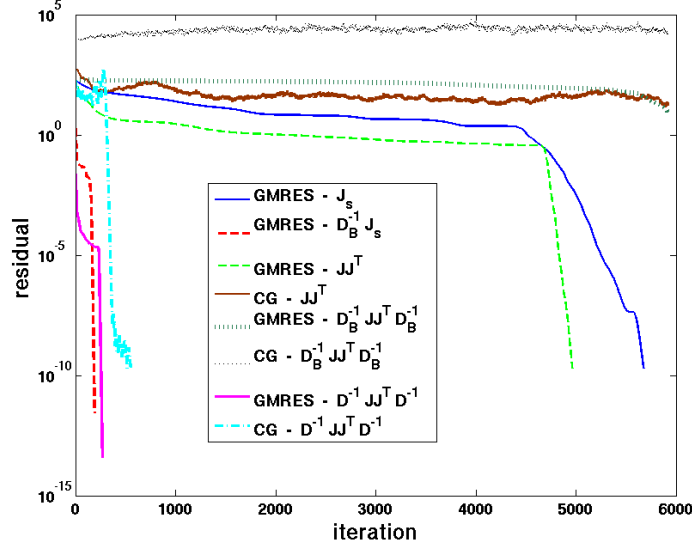


Figure 10: Typical convergence behavior of GMRES and CG for the problem at hand. Suitable convergence behavior results for GMRES with $D_B^{-1}J_s$ as coefficient matrix, and for GMRES or CG with $D^{-1}JJ^TD^{-1}$ as coefficient matrix. However, the only viable option for our problem is the GMRES method with $D_B^{-1}J_s$ as coefficient matrix.

terminated Jacobian matrix of the system (36), J_s represents a square, non-singular matrix composed of a subset of columns of J , the preconditioner D_B is the Jacobian matrix of the terms in (36) linear in the unknowns $\{\hat{a}_{m,n}\}$, with columns corresponding to the derivatives with respect to the real and imaginary parts of the coefficients $\{\hat{a}_{m,n}\}$ (it is a block diagonal matrix), and the preconditioner D is a diagonal matrix having the diagonal elements of JJ^T on its diagonal. As can be seen from Figure 10, suitable convergence behavior results only from the use of GMRES with $D_B^{-1}J_s$ as coefficient matrix (i.e., the use of GMRES to solve linear systems with J_s as coefficient matrix and D_B as a preconditioner), as well as from using GMRES or CG with $D^{-1}JJ^TD^{-1}$ as coefficient matrix (i.e., the use of GMRES or CG to solve linear systems with JJ^T as coefficient matrix and D as a preconditioner).

The block diagonal preconditioner D_B is very effective when used with the GMRES method to solve linear systems with J_s as coefficient matrix, as seen in Figure 10. For the example depicted, it took 190 iterations to solve for a system having 5,925 unknowns. The corresponding run with unpreconditioned GMRES required 5,676 iterations, making it impractical for our purposes. Using the preconditioner D and both the GMRES and CG methods to solve for systems having JJ^T as coefficient matrix also gave good results. For the example in Figure 10, these two methods took, respectively, 269 and 552 iterations

to solve the preconditioned system. However, per the discussion in Section 3.2, the block diagonal preconditioner D_B is readily available and easy to manipulate, whereas assembling the preconditioner D requires calculating the diagonal terms of the matrix JJ^T , and these terms are not readily available for our problem. Therefore, the only viable option for us is the use of the GMRES method with preconditioner D_B to solve systems having J_s as the coefficient matrix. As a result, the computation of the minimum norm solution z directly from (48)–(49) is unfeasible for the problem at hand.

Returning to the linear system in (48), we thus express J as composed by two matrices,

$$J = [J_s \mid J_r], \quad (50)$$

where J_s has dimension $p \times p$ (and is non-singular) and J_r has dimension $p \times (q-p)$. Now we consider the system $J_s^{-1}Jz = J_s^{-1}b$ obtained by multiplying (48) with J_s^{-1} , yielding

$$[I \mid J_s^{-1}J_r]z = J_s^{-1}b, \quad (51)$$

where I is the $p \times p$ identity matrix. We work directly with the system (51) and compute the desired solution z by solving two sub-problems, namely:

1. Compute the right-hand side $J_s^{-1}b$, as well as the $q-p$ columns of the submatrix $J_s^{-1}J_r$ of the coefficient matrix $[I \mid J_s^{-1}J_r]$ in (51). This sub-problem will therefore require the solution of $q-p+1$ linear systems having J_s as coefficient matrix. It will be feasible if solving linear systems having J_s as coefficient matrix can be done efficiently and if $q-p+1$ is small. Both of these requirements are satisfied in our study since first, per the discussion from the previous paragraphs, we can use the GMRES method to solve the required linear systems efficiently, and second, for our problem, $q-p = 3$ due to the 3-tuple (φ, S, T) of additional unknowns in the problem formulation.
2. Upon completion of sub-problem 1, compute the minimum norm solution given by the Moore-Penrose inverse for the underdetermined system of linear equations (51).

Per sub-problem 1 above, one first needs to solve $k = 1, \dots, q-p+1$ linear systems

$$J_s \tilde{z}_k = \tilde{b}_k, \quad (52)$$

where, for $k = 1, \dots, q-p$, the k -th linear system (52) will have the right-hand side vector \tilde{b}_k equal to the k -th column of the matrix J_r , so that the solutions \tilde{z}_k of said $q-p$ linear systems yield the columns of the submatrix $J_s^{-1}J_r$ of the coefficient matrix $[I \mid J_s^{-1}J_r]$ in (51). The solution of the remaining linear system (52), with $\tilde{b}_{q-p+1} = b$, yields the right-hand side $J_s^{-1}b$ in (51). Solving these $q-p+1$ linear systems (52) is not an obstacle since they can be solved either independently, in parallel, or with an implementation of a (direct or

iterative) solver for linear systems that handles multiple right-hand sides. Recall that the viable option for us is to use the GMRES method for linear systems. In our implementation, we combined it with the use of POSIX threads (pthreads) programming [27] in order to solve the required linear systems (52) in parallel. Hence, in the current study, the solution of the $q-p+1 = 4$ linear systems (52) having J_s as coefficient matrix was achieved basically in the same amount of time as that required to solve a single such system.

Upon completion of sub-problem 1, what remains to be done is to compute the minimum norm solution z from the system in (51). As previously noted, one desirable property for fast convergence of the GMRES method is for the eigenvalues of the coefficient matrix to be clustered around a few values, away from zero, since, typically, the number of iterations required for convergence when using the GMRES method depends on the number of distinct eigenvalues of the coefficient matrix of the linear system [16]. Thus, we also used the GMRES method to solve for the minimum norm solution z in (51), since this requires solving a linear system having

$$I + (J_s^{-1}J_r)(J_s^{-1}J_r)^T \quad (53)$$

as coefficient matrix, and the matrix (53) has all but $q-p$ eigenvalues equal to one, with the remaining eigenvalues greater than or equal to one. (Recall that J_s is a non-singular $p \times p$ matrix and J_r has dimension $p \times (q-p)$, where $p < q$.) This follows from the fact that the eigenvalues λ and eigenvectors y of the matrix (53) satisfy

$$(J_s^{-1}J_r)(J_s^{-1}J_r)^T y = (\lambda - 1)y. \quad (54)$$

Noting that the null space of the matrix $(J_s^{-1}J_r)^T$ has dimension (at least) $p - (q-p) = 2p-q$, it follows that the matrix $(J_s^{-1}J_r)(J_s^{-1}J_r)^T$ has zero as an eigenvalue, that is, $\lambda = 1$, with multiplicity (at least) $2p-q$. Furthermore, $(J_s^{-1}J_r)(J_s^{-1}J_r)^T$ is positive semi-definite and symmetric, so its eigenvalues $(\lambda-1)$ in (54) are non-negative and, thus, the remaining (at most) $q-p$ eigenvalues of the matrix (53) satisfy $\lambda \geq 1$. The significance here is that solving a linear system with the matrix (53) as coefficient matrix, which is required in order to compute the minimum norm solution z of system (51), should take $q-p+1$ iterations if we use the GMRES method. For our problem, this means $q-p+1 = 4$ iterations. Note also that computing matrix-vector products with the matrix (53) can be easily done (since the $q-p = 3$ columns of the matrix $J_s^{-1}J_r$ have been previously computed and stored in memory). Furthermore, no preconditioning is required to solve linear systems having (53) as coefficient matrix. Hence, using the GMRES method to solve the aforementioned sub-problem 2 poses no difficulty and results in a negligible amount of additional computing time when solving for the Newton step using the proposed approach.

Finally, and denoting the system (36) as $\mathbf{F} = \mathbf{0}$, note that the vector b in (51) corresponds to $-\mathbf{F}$ evaluated at the current solution estimate (from Newton's method). Also, based on our presentation of the material, it may seem natural to consider the matrix $J_{\hat{\mathbf{a}}}$ introduced in Section 3.2, whose columns correspond to derivatives of \mathbf{F} with respect to the real and imaginary parts of the unknowns $\{\hat{a}_{m,n}\}$, as that corresponding to the matrix J_s in (50)–(51). Recall, though, that $J_{\hat{\mathbf{a}}}$ is singular at a solution of $\mathbf{F} = \mathbf{0}$. We therefore define the matrix J_s as that obtained by replacing three columns from $J_{\hat{\mathbf{a}}}$ by the columns of the Jacobian matrix of \mathbf{F} corresponding to derivatives with respect to the unknowns φ , S , and T . This proved effective in dealing with said singularity when computing the Newton step from the corresponding system (51) during the numerical continuation. (As discussed in [26], the kernel of the Jacobian matrix at a solution of $\mathbf{F} = \mathbf{0}$ is typically three-dimensional.) The replaced columns from $J_{\hat{\mathbf{a}}}$ define the columns of the matrix J_r in (50), which are needed to construct the matrix $J_s^{-1}J_r$ in (51). These three columns can be computed (efficiently) via matrix-vector products of the Jacobian matrix (see Section 3.2) and standard basis vectors.

References

- [1] Eugene L. Allgower and Kurt Georg. *Introduction to Numerical Continuation Methods*. Classics in Applied Mathematics. SIAM, 2003.
- [2] Igor S. Aranson and Lorenz Kramer. The world of the complex Ginzburg-Landau equation. *Rev. Mod. Phys.*, 74:99–143, 2002.
- [3] Philip J. Aston and Carlo R. Laing. Symmetry and chaos in the complex Ginzburg-Landau equation. I. Reflectional symmetries. *Dynam. Stability Systems*, 14:233–253, 1999.
- [4] Philip J. Aston and Carlo R. Laing. Symmetry and chaos in the complex Ginzburg-Landau equation. II. Translational symmetries. *Physica D*, 135:79–97, 2000.
- [5] Michele Bartuccelli, Peter Constantin, Charles R. Doering, John D. Gibbon, and Magnus Gisselgård. On the possibility of soft and hard turbulence in the complex Ginzburg-Landau equation. *Phys. D*, 44(3):421–444, 1990.
- [6] Adi Ben-Israel and Thomas N.E. Greville. *Generalized Inverses : Theory and Applications*. Springer-Verlag, 2003.

- [7] G. Benettin, L. Galgani, A. Giorgilli, and J.-M. Strelcyn. Lyapunov characteristic exponents for smooth dynamical systems and for Hamiltonian systems; A method for computing all of them. Part I: Theory. *Meccanica*, 15:9–20, 1980.
- [8] Lutz Brusch, Alessandro Torcini, Martin van Hecke, Martín G. Zimmermann, and Markus Bär. Modulated amplitude waves and defect formation in the one-dimensional complex Ginzburg-Landau equation. *Physica D*, 160:127–148, 2001.
- [9] Gary J. Chandler and Rich R. Kerswell. Invariant recurrent solutions embedded in a turbulent two-dimensional Kolmogorov flow. *J. Fluid Mech.*, 722:554–595, 2013.
- [10] P. Cvitanović, R. Artuso, P. Dahlenqvist, R. Mainieri, G. Tanner, G. Vattay, N. Whelan, and A. Wirzba. *Chaos: Classical and Quantum*. 2014. Webbook available at chaosbook.org.
- [11] Arjen Doelman. Slow time-periodic solutions of the Ginzburg-Landau equation. *Physica D*, 40:156–172, 1989.
- [12] Arjen Doelman and Edriss S. Titi. Regularity of solutions and the convergence of the Galerkin method in the Ginzburg-Landau equation. *Numer. Funct. Anal. Optim.*, 14(3-4):299–321, 1993.
- [13] M. Frigo and S. G. Johnson. FFTW: An adaptive software architecture for the FFT. In *ICASSP Conference Proceedings*, volume 3, pages 1381–1384, 1998. <http://www.fftw.org/>.
- [14] Gene H. Golub and Charles F. Van Loan. *Matrix Computations*. The Johns Hopkins University Press, 1996.
- [15] Martin Golubitsky, Ian Stewart, and David A. Schaeffer. *Singularities and Groups in Bifurcation Theory. Volume II*. Applied Mathematical Sciences. Springer-Verlag, 1988.
- [16] Anne Greenbaum. *Iterative Methods for Solving Linear Systems*. Frontiers in Applied Mathematics. SIAM, 1997.
- [17] Philip Holmes. Spatial structure of time-periodic solutions of the Ginzburg-Landau equation. *Physica D*, 23:84–90, 1986.
- [18] M. S. Jolly, R. Temam, and C. Xiong. Convergence of a chaotic attractor with increased spatial resolution of the Ginzburg-Landau equation. *Chaos Solitons Fractals*, 5(10):1833–1845, 1995.

- [19] Todd Kapitula and Stanislaus Maier-Paape. Spatial dynamics of time-periodic solutions for the Ginzburg-Landau equation. *Zeitschrift für Angewandte Mathematik und Physik*, 47:265–305, 1996.
- [20] Laurence R. Keefe. Dynamics of perturbed wavetrain solutions to the Ginzburg-Landau equation. *Stud. Appl. Math.*, 73(2):91–153, 1985.
- [21] Bernd Krauskopf, Hinke M. Osinga, and Jorge Galán-Vioque, editors. *Numerical Continuation Methods for Dynamical Systems: Path Following and Boundary Value Problems*. Understanding Complex Systems. Springer, 2007.
- [22] Y. A. Kuznetsov. *Elements of Applied Bifurcation Theory*. Springer-Verlag, 1998.
- [23] Y. Lan. Cycle expansions: From maps to turbulence. *Commun Nonlinear Sci Numer Simulat*, 15:502–526, 2010.
- [24] C. David Levermore and Marcel Oliver. The complex Ginzburg-Landau equation as a model problem. In *Dynamical Systems and Probabilistic Methods in Partial Differential Equations*, volume 31 of *Lectures in Appl. Math.*, pages 141–190. Amer. Math. Soc., Providence, RI, 1996.
- [25] D. J. B. Lloyd, A. R. Champneys, and R. E. Wilson. Robust heteroclinic cycles in the one-dimensional complex Ginzburg-Landau equation. *Physica D*, 204:240–268, 2005.
- [26] Vanessa López, Philip Boyland, Michael T. Heath, and Robert D. Moser. Relative periodic solutions of the complex Ginzburg-Landau equation. *SIAM J. Appl. Dyn. Syst.*, 4(4):1042–1075, 2005.
- [27] Linux Programmer’s Manual. POSIX threads programming. <http://man7.org/linux/man-pages/man7/pthreads.7.html>.
- [28] A. Mielke. The Ginzburg-Landau equation in its role as a modulation equation. In *Handbook of Dynamical Systems, Vol. 2*, B. Fiedler, ed., pages 759–834. Elsevier Science, 2002.
- [29] Willard Miller, Jr. *Symmetry Groups and Their Applications*. Academic Press, Inc., 1972.
- [30] H. T. Moon, P. Huerre, and L. G. Redekopp. Transitions to chaos in the Ginzburg-Landau equation. *Phys. D*, 7(1-3):135–150, 1983.

- [31] Peter J. Olver. *Equivalence, Invariants, and Symmetry*. Cambridge University Press, 1995.
- [32] J. M. Ortega and W. C. Rheinboldt. *Iterative Solution of Nonlinear Equations in Several Variables*. Classics in Applied Mathematics. SIAM, 2000.
- [33] Edward Ott. *Chaos in Dynamical Systems*. Cambridge University Press, 2002.
- [34] Y. Saad and M. H. Schultz. GMRES: A generalized minimal residual algorithm for solving nonsymmetric linear systems. *SIAM J. Sci. Stat. Comput.*, 7:856–869, 1986.
- [35] A. G. Salinger, M. Bou-Rabee, R. P. Pawlowski, E. D. Wilkes, E. A. Burroughs, R. B. Lehoucq, and L. A. Romero. LOCA: A library of continuation algorithms - theory and implementation manual. Technical report, Sandia National Laboratory, 2001. <http://www.cs.sandia.gov/projects/loca/index.html>.
- [36] David E. Stewart and Zbigniew Leyk. Meschach library. Technical report, Australian National University, 1994. <http://www.netlib.org/c/meschach/readme>.
- [37] Peter Takáč. Bifurcations to invariant 2-tori for the complex Ginzburg-Landau equation. *Appl. Math. Comput.*, 89:241–257, 1998.
- [38] Roger Temam. *Infinite-dimensional Dynamical Systems in Mechanics and Physics*, volume 68 of *Applied Mathematical Sciences*. Springer-Verlag, New York, 1997.
- [39] Martin van Hecke. Coherent and incoherent structures in systems described by the 1D CGLE: Experiments and identification. *Physica D*, 174:134–151, 2003.
- [40] W. van Saarloos. The complex Ginzburg-Landau equation for beginners. In *Spatio-Temporal Patterns in Nonequilibrium Complex Systems*, P. E. Cladis and P. Palffy-Muhoray, eds., Studies in the Sciences of Complexity, Proceedings XXI. Addison-Wesley, Reading, MA, 1994.
- [41] Claudia Wulff and Andreas Schebesch. Numerical continuation of symmetric periodic orbits. *SIAM J. Appl. Dyn. Syst.*, 5(3):435–475, 2006.